npj | science of food

Article

Published in partnership with Beijing Technology and Business University & International Union of Food Science and Technology

https://doi.org/10.1038/s41538-025-00633-2

The *Artemisia argyi* oil reduces high-fat diet-induced obesity by enhancing thermogenesis in brown adipose tissue

Shuai Wang[1,2,8], ShengLan Lin[3,8], Fuan Xie[4,8], Shuting Liu[5], Ting He[5], Kun Chen[5], Zhengrong Huang[1], Wenlong Xie[5], Hongqiu Cheng[2], Jian Zhang[6,7] ✉ & Weihua Li[1] ✉

Amid growing global concerns over obesity, the identification of novel lipid resources with potential health benefits has become a key focus in food science. *Artemisia argyi*, a traditional edible plant, is valued for its bioactive volatile oils, yet the effects of *Artemisia argyi* oil (AAO) on lipid metabolism and energy balance remain largely unexplored. Brown adipose tissue (BAT), which facilitates energy dissipation via non-shivering thermogenesis, is a key target for dietary strategies to combat obesity. Here, we demonstrate that AAO combats obesity by promoting BAT thermogenesis, resulting in significant reductions in weight gain, body fat, and improved insulin sensitivity. Mechanistically, AAO promotes Ucp1 transcription by directly activating ZFP516 expression and enhancing its interaction with LSD1. These findings identify AAO as a natural dietary component with potential to improve metabolic health through BAT activation, offering insights for its use in functional foods aimed at energy balance and weight management.

The rising prevalence of obesity and associated metabolic disorders has spurred global interest in dietary strategies to support energy balance and healthy weight management[1,2]. Obesity is closely linked to diseases such as type II diabetes, hypertension, cardiovascular conditions, certain cancers, osteoarthritis, fatty liver[3–5]. Adipose tissue plays a crucial role in maintaining metabolic homeostasis and is typically categorized into three types: white adipose tissue (WAT), beige adipose tissue, and BAT[6,7]. WAT predominantly stores excess energy as triglycerides (TG), whereas BAT and beige adipose tissue dissipate energy to reduce TG accumulation during high-fat diet (HFD) feeding[8,9]. BAT is rich in mitochondria, with uncoupling protein-1 (UCP1) located in the mitochondrial inner membrane, where it catalyzes proton leakage to generate heat instead of ATP[10–12]. Studies have shown that human BAT activity is associated with a reduction in body weight, and promoting the thermogenic function of BAT may offer an effective strategy for combating obesity and metabolic diseases[13,14]. Transcriptional regulators, such as peroxisome proliferator-activated receptor-gamma coactivator-1 alpha (PGC-1α), Zinc finger protein 516 (ZFP516), lysine-specific demethylase 1 (LSD1), and PR domain-containing protein 16 (PRDM16), play essential roles in regulating the thermogenic function of BAT[15–17]. ZFP516, a cold-inducible transcription factor enriched in BAT, promotes the transcription of UCP1 and other BAT-enriched genes to drive non-shivering thermogenesis and has emerged as a potential target for obesity treatment[17,18].

Driven by the growing emphasis on sustainable development and the rise in health-conscious consumption demands, plant-based ingredients have emerged as a cutting-edge focus in food innovation[19]. *Artemisia argyi*, a traditional edible plant widely favored in East Asian cuisine, has seen its leaves commonly used in local specialties such as green rice cakes and herbal teas[20,21]. In recent years, it has also demonstrated unique value in the development of functional baked goods, plant-based beverages, and dietary supplements[22]. *Artemisia argyi* is rich in bioactive compounds such as polysaccharides, flavonoids, and volatile oils[20]. *Artemisia argyi* extract

[1]Department of Cardiology, Xiamen Key Laboratory of Cardiac Electrophysiology, Xiamen Institute of Cardiovascular Diseases, The First Affiliated Hospital of Xiamen University, School of Medicine, Xiamen University, Xiamen, China. [2]Department of Hepatology and Infectious Diseases, The Second Affiliated Hospital of Shantou University Medical College, Shantou, Guangdong, PR China. [3]Department of Gerontology, The First Affiliated Hospital of Xiamen University, School of Medicine, Xiamen University, Xiamen, China. [4]Cancer Research Center, Xiang'an Hospital of Xiamen University, School of Medicine, Xiamen University, Xiamen, Fujian, PR China. [5]State Key Laboratory of Cellular Stress Biology, Innovation Center for Cell Signaling Network and Engineering Research Center of Molecular Diagnostics of the Ministry of Education, School oF Life Sciences, Xiamen university, Xiamen, Fujian, China. [6]Shandong Key Laboratory of Healthy Food Resources Exploration and Creation, Qilu University of Technology (Shandong Academy of Sciences), Jinan, China. [7]School of Food Science and Engineering, Qilu University of Technology (Shandong Academy of Sciences), Jinan, China. [8]These authors contributed equally: Shuai Wang, ShengLan Lin, Fuan Xie.
✉e-mail: 7210201081@stu.jiangnan.edu.cn; liweihua@xmu.edu.cn

demonstrates significant therapeutic efficacy in the treatment of both acute and chronic gastritis, effectively ameliorating gastric mucosal erosion and alleviating gastrointestinal symptoms, while exhibiting favorable safety and tolerability profiles in patients[23]. *Artemisia argyi* oil (AAO), which contains cineole and camphor, exhibits outstanding lipid solubility, thermal stability, and broad-spectrum antimicrobial properties[24,25]. These attributes have enabled its successful application in lipid-based food preservation systems and flavor enhancement. At a gavage dose of 500 mg/kg, mice showed no changes in behavior or weight, and no macroscopic abnormalities were observed in any organs, indicating the high safety profile of AAO[26]. Additionally, research indicates that water-soluble extracts from *Artemisia argyi* can modulate lipid metabolism in high-fat diet models, reducing lipid accumulation in adipocytes[21]. Furthermore, AAO can enhance hepatic fatty acid β-oxidation efficiency, underscoring its potential to improve food quality and promote health[27]. However, the effects and mechanisms of AAO in BAT thermogenesis and energy homeostasis regulation, a critical aspect of lipid catabolism, remain insufficiently explored. Investigating the interactions between AAO and BAT-specific pathways is of great significance for fully unlocking its potential as a novel functional lipid component in metabolism-oriented food formulations.

In this study, we examined the effects of orally administered AAO in conjunction with a HFD on obesity and metabolic dysfunction in mice. AAO treatment effectively mitigated HFD-induced obesity, significantly reducing body fat percentage, serum triglycerides, free fatty acids, and total cholesterol levels, while improving metabolic function in mice. Mechanistically, AAO activated ZFP516 expression in BAT, which in turn enhanced UCP1 expression. Moreover, AAO strengthened the interaction between ZFP516 and LSD1, further promoting UCP1 expression in BAT. Our findings highlight the therapeutic potential of AAO in combating obesity and metabolic disorders.

Results

Extraction, pharmacokinetics, and toxicological analysis of AAO

The hydrodistillation of *Artemisia argyi* leaves using a Clevenger apparatus yielded 0.96% (w/w) of essential oil on a dry weight basis, consistent with previously reported ranges of 0.5–1.5% for this species. GC-MS analysis identified 15 major volatile compounds in the extracted essential oil, accounting for 91.65% of the total peak area (Table 1, Fig. S1). Monoterpenoids were the predominant constituents, representing over 80% of the composition, including cineole, camphor, and α-thujone (Table 1). Additionally, β-caryophyllene and 1-octen-3-ol were also identified as significant components. These results are closely aligned with previous literature reports, with minor compositional variations likely attributable to geographic or genetic influences on phytochemical profiles[28].

Table. 1 | AAO component analysis by GC-MS

Peak number	Rt (min)	Compound	mf	Peak area (%)
1	6.22	Camphene	C10H16	2.93
2	7.15	1-Octen-3-ol	C8H16O	2.20
3	8.48	o-Cymene	C10H14	0.42
4	8.74	Cineole	C10H18O	35.95
5	9.86	γ- Terpinene	C10H16	2.04
6	10.12	Cyclohexanol	C6H12O	2.71
7	11.38	α1-(-)-Thujone	C10H16O	11.05
8	11.71	(+)-Thujone	C10H16O	0.96
9	12.87	Camphor	C10H16O	14.66
10	13.61	(−)-Borneol	C10H18O	10.50
11	13.85	Terpinen-4-ol	C10H18O	2.21
12	14.39	α-Terpineol	C10H16	1.63
13	15.2	(E)-Carveol	C10H16O	0.71
14	17.33	Bornyl acetate	C12H20O2	0.90
15	21.43	β-Caryophyllene	C15H24	2.79

Cineole is one of the major components of AAO and is known to possess significant biological activity, making it a suitable marker for reflecting the pharmacokinetic behavior of AAO in vivo[26]. As shown in Table S1 and Fig. S2A, the mean $AUC_{0\text{-}t}$, C_{max}, and T_{max} values were 18.87 ± 1.87 μg/l*h, 6.18 ± 0.54 μg/l, and 1 h, respectively, following oral administration of AAO (500 mg/kg) to rats. Additionally, the plasma elimination half-life ($t_{1/2}$) and mean residence time ($MRT_{0\text{-}t}$) were 3.72 ± 0.68 h and 2.98 ± 0.35 h, respectively. Furthermore, liver exposure results indicated that 1 h after oral administration of 500 mg/kg AAO, the maximum concentration of cineole in the liver reached approximately 4.8 μg/g (Fig. S2B).

Prior to exploring the anti-obesity effects in vivo, a toxicity study of AAO was conducted in mice on NCD. As shown in Fig. S3A, AAO did not affect the survival rate of mice. The liver injury markers (alanine aminotransferase (ALT), aspartate aminotransferase (AST), alkaline phosphatase (ALP)), kidney injury markers (blood urea nitrogen (BUN), creatinine), and myocardial injury markers (cardiac troponin T (cTnT), cardiac troponin I (cTnI), B-type natriuretic peptide (BNP)) in the serum of mice were all unaffected by AAO (Fig. S3B–I). AAO also did not affect the activity level of mice (Fig. S3J). We further examined the muscle phenotype in the AAO oral group, but no apparent defects were observed (Fig. S3K). Furthermore, we also evaluated the toxicity of AAO in vitro. As shown in Fig. S3L–O, AAO did not significantly affect the proliferation of hepatocytes (LX2), renal cells (HK-2), cardiomyocytes (H9c2), or skeletal muscle cells (C2C12). These results suggest that AAO does not exhibit significant toxicity either in vivo or in vitro.

AAO effectively counteracts obesity induced by HFD

We first compared the effects of AAO with established obesity treatments, including pharmaceutical interventions (GLP-1 analogs) and well-characterized plant-based thermogenic agents (capsaicin), in combating high-fat diet-induced obesity (Fig. S4A).

At week 23, body weight and body fat percentage were significantly reduced in the semaglutide, capsaicin, and AAO groups (Fig. S4B–C). And mice in the oral AAO group exhibited lower body weight and body fat percentage compared to those in the oral capsaicin group, while mice in the semaglutide group had lower body weight and body fat percentage than those in the AAO group (Fig. S4B–C). Additionally, serum levels of TG, non-esterified fatty acids (NEFA), and total cholesterol (T-CHO) in the AAO group were significantly lower than those in the capsaicin group (Fig. S4D–F). However, serum T-CHO levels in the AAO group were significantly higher than those in the semaglutide group (Fig. S4F). Furthermore, mice in the AAO group exhibited glucose tolerance and insulin sensitivity similar to those in the semaglutide group (Fig. S4G–J). Finally, we found that the rectal temperature of mice in the AAO and capsaicin groups was approximately 38 °C at room temperature (RT). However, under acute cold stimulation, the rectal temperature of mice in the AAO group was higher than that of mice in the capsaicin group (Fig. S4K–M). Based on these findings, we selected AAO for a comprehensive investigation.

To further evaluate the effects of different concentrations of AAO on body weight in mice, we administered low, medium, and high concentrations of AAO via gavage in conjunction with HFD and monitored body weight weekly for each group (Fig. 1A). As shown in Fig. 1B, an increase in AAO concentration resulted in a slower rate of body weight gain compared to the HFD group. At week 12, the body weight of mice in the HA group was approximately 6 g less than that of mice in the HFD group (Fig. 1B). Further analysis of body composition showed that increasing concentrations of AAO progressively decreased fat mass (Fig. 1C, D). Simultaneously, we assessed the serum concentrations of TG, NEFA, and T-CHO. Serum TG, NEFA, and T-CHO levels were significantly lower in the MA and HA groups compared to the HFD group (Fig. 1E–G). However, there was no difference in T-CHO levels between the LA group and the HFD group mice (Fig. 1G). To further evaluate the effect of AAO on liver function, we

measured serum levels of AST and ALT. As shown in Fig. S5A, B, serum AST and ALT levels decreased gradually with increasing concentrations of AAO. However, low-concentration AAO did not significantly reduce AST levels compared to the HFD group (Fig. S5A). Additionally, serum LDL levels decreased in a dose-dependent manner with AAO treatment compared to the HFD group (Fig. S5C). Moreover, mice in the HFD group exhibited more severe glucose intolerance and insulin resistance than those on the NCD (Fig. 1H–K). Simultaneously, both medium and high concentrations of AAO improved insulin sensitivity and alleviated glucose intolerance (Fig. 1H–K). These findings suggest that AAO effectively counteracts obesity and improves insulin sensitivity in HFD.

AAO effectively reduces lipid accumulation in adipose tissue and the liver

Considering the significant reduction in body fat percentage with AAO, we further examined the adipose tissue and liver weights in each group of mice. As depicted in Fig. 2A–D, the weights of iWAT, gWAT, BAT, and liver in the MA and HA groups were notably lower compared to the HFD group. However, there were no significant differences in iWAT and liver weights between the LA and HFD groups (Fig. 2A–D). Further H&E staining analysis showed that AAO effectively reduced lipid accumulation in adipocytes and hepatocytes, especially at higher concentrations (Fig. 2E). Moreover, TG content measurements were consistent with the H&E staining results, indicating that TG levels in adipose and liver tissues of mice in the HA group were significantly lower than those in the HFD group (Fig. 2F–I). Overall, these findings demonstrated that AAO effectively reduced lipid and TG accumulation in the adipose tissues and liver of mice fed a high-fat diet.

AAO significantly facilitates thermogenesis of mice

Previous studies have shown that enhanced thermogenic capacity of BAT can significantly counteract obesity induced by HFD[29,30]. To investigate whether AAO can enhance BAT thermogenesis, we measured the core body temperature of mice in each group under both RT and acute cold exposure (Fig. 3A). As shown in Fig. 3B, C, after 4 h of cold exposure at 4 °C, the body temperature drop was significantly smaller in the MA and HA groups compared to the HFD group. In contrast, mice treated with low-concentration AAO did not show resistance to the cold-induced drop in body temperature (Fig. 3B, C). Meanwhile, under RT conditions, the core body temperature of all groups remained stable at approximately 38 °C, with no significant differences observed (Fig. 3B). To further investigate the impact of AAO on systemic metabolism in mice, we measured oxygen consumption and heat production across all groups using a metabolic cage system. As depicted in Fig. 3D, E, the administration of AAO did not alter the food intake or physical activity of the mice. However, it led to a significant increase in both oxygen consumption and heat production, observed during both the day and night, when compared to the HFD group (Fig. 3F–I). Notably, oral administration of low-concentration AAO had no effect on oxygen consumption and heat production in mice, either during the day or at night, compared to the HFD group (Fig. 3F–I). Taken together, these results suggest that AAO notably enhances thermogenesis and energy expenditure in mice.

AAO is essential for promoting the expression of thermogenic genes

Considering the enhanced capacity of AAO-treated mice to sustain body temperature under acute cold exposure, we focused on examining the influence of AAO on BAT. To further explore the impact of AAO on BAT thermogenic function, we performed RNA-seq on BAT samples from mice in both the HFD and HA groups. A clear separation was observed between the HFD and HA groups, indicating substantial differences in gene expression profiles (Fig. 4A). As shown in Fig. 4B, the HA group displayed 2284 upregulated genes and 990 downregulated genes compared to the HFD group. We further performed heatmap analysis on the genes that were either upregulated or downregulated. As depicted in Fig. 4C, the upregulated genes are predominantly involved in thermogenic processes (such as *Ucp1*, *Dio2*, *Zfp516*, and *Elovl3*) and oxidative phosphorylation (including *Cox8b*, *Ndufa3*, and *Atp5e*). Conversely, the downregulated genes are primarily associated with lipid biosynthesis (such as *Fasn*, *Fads6*, *Scd1*, and *Acly*) and pathways related to inflammation (including *Nfkb1*, *Il6*, *Ccr1*, and *Tnfα*) (Fig. 4C). Functional enrichment analysis of the upregulated genes identified significant overrepresentation of pathways involved in thermogenesis, oxidative phosphorylation, fatty acid metabolism, and TCA cycle (Fig. 4D). In contrast, the downregulated genes were predominantly associated with the inflammatory response, NF-kappa B signaling pathway, and lipid biosynthesis (Fig. 4E). These results suggest that AAO enhances the expression of thermogenic genes in BAT while concurrently inhibiting the expression of genes involved in lipid synthesis.

AAO enhances the expression of thermogenic and oxidative phosphorylation genes in BAT

To further validate the results obtained from RNA-seq analysis, we performed experimental validation by collecting BAT tissues from the NCD, HFD, LA, MA, and HA groups, followed by western blot, immunofluorescence, and qPCR analyses. The expression level of UCP1 in the BAT of mice in the HFD group was significantly lower than that in the NCD group, indicating the successful establishment of the mouse model (Fig. 5A and S6A). As the AAO concentration increased, the protein levels of UCP1, PGC1α, PPARα, and PRDM16 in BAT were elevated, while AGT levels decreased (Fig. 5A and S6A, B). The qPCR data further corroborated the results obtained from the western blot analysis (Fig. 5B–F). Furthermore, the immunofluorescence results provided additional confirmation of the alterations in UCP1 protein expression levels (Fig. 5G).

PGC-1α is a key regulator of mitochondrial biogenesis and function, playing a crucial role in regulating mitochondrial density and oxidative metabolism in BAT[31–33]. The increased expression of PGC1α in AAO-treated mice prompted us to investigate whether AAO also affects genes involved in mitochondrial oxidative phosphorylation and mitochondrial content in BAT. As shown in Fig. 5H and Fig. S6C, AAO feeding effectively enhanced the protein expression levels of COXII and COXIV in BAT, particularly at the higher concentration of AAO. Furthermore, the mRNA levels of *Cox8b* and *Cox5b* in the BAT of MA and HA groups were significantly higher than those in the HFD group, while the expression levels in the LA and HFD groups were comparable (Fig. 5I–J). Meanwhile, the protein expression levels of Tom20, a mitochondrial marker, remained comparable across all groups of mice (Fig. S7A). Additionally, qPCR results indicated that AAO did not affect mitochondrial content (Fig. S7B). In summary, AAO promoted the expression of thermogenic and oxidative phosphorylation genes in BAT in vivo.

AAO upregulates lipolysis-related genes and downregulates genes associated with inflammation and lipogenesis in BAT in vivo

To investigate the effect of AAO on lipolysis in BAT, we evaluated the expression of ATGL and HSL at both the protein and mRNA levels. As illustrated in Fig. 6A–C and Fig. S8A, the expression of HSL and ATGL was significantly elevated in the MA and HA groups compared to the HFD group. Previous studies have suggested that the "whitening" of BAT is associated with increased lipogenesis and inflammation within this tissue[34]. To further explore this, we assessed the expression of lipogenesis-related genes, including acetyl-CoA carboxylase (ACC) and fatty acid synthase (FASN), in the BAT of mice from all groups. As shown in Fig. 6A, D, E, and Fig. S8A, increasing the AAO concentration progressively reduced the expression levels of ACC and FASN in BAT. Additionally, we examined the expression of key inflammatory markers, including tumor necrosis factor-alpha (TNFα) and interleukin-6 (IL6), in BAT across all experimental groups. AAO effectively diminished the expression of both IL6 and TNFα (Fig. S9A–D). Taken together, these findings suggest that AAO enhances lipolysis, and inhibits the expression of genes associated with inflammation and lipogenesis.

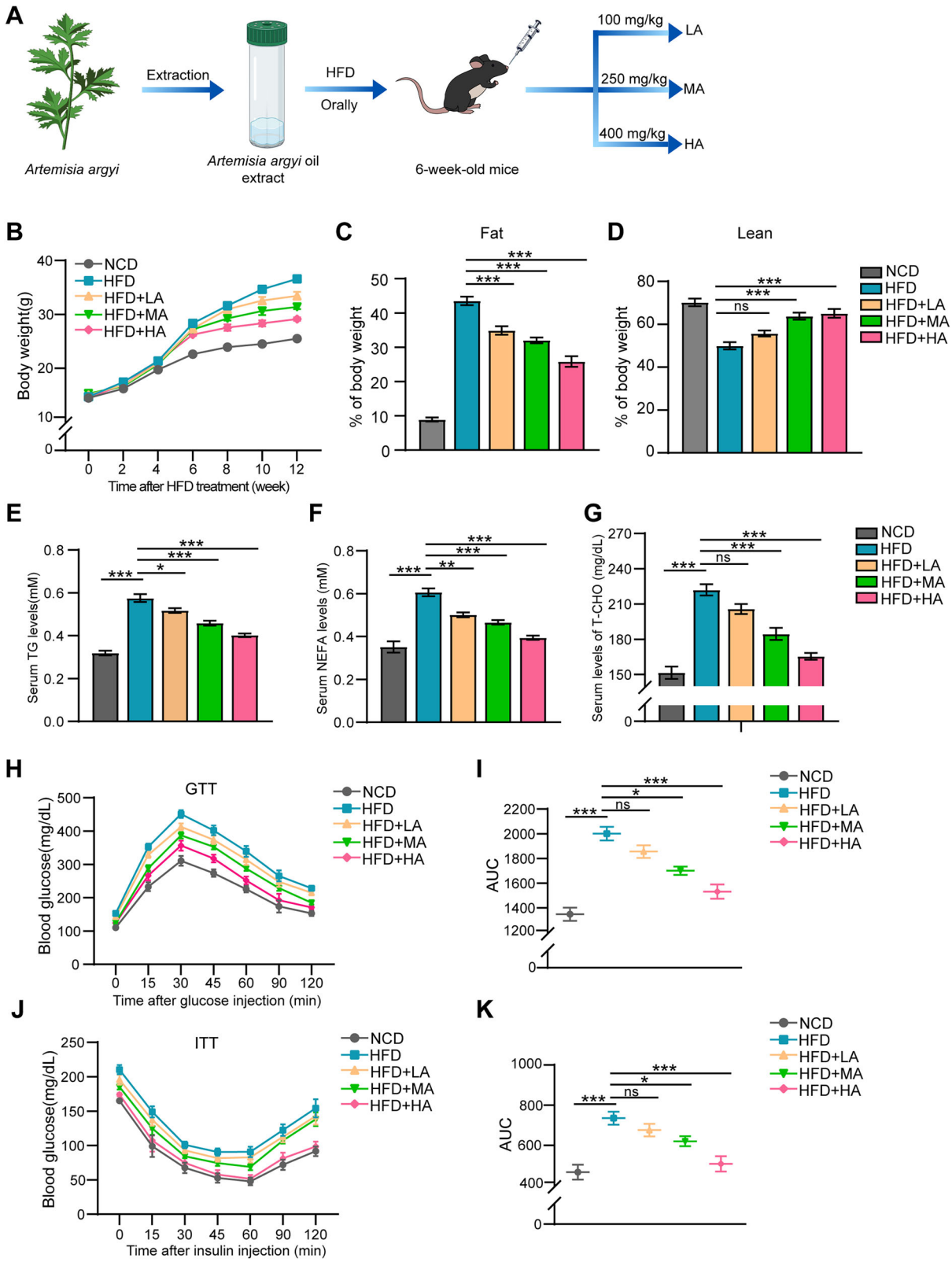

Fig. 1 | AAO effectively mitigates obesity induced by HFD. A The figure illustrates the isolation and extraction of AAO, followed by oral administration to mice. **B** The body weight of mice in each group (n = 6). At week 10.5, the average fat (**C**) and lean (**D**) mass of the mice were evaluated using the Echo MRI composition analyzer (n = 6). In week 12, TG (**E**), NEFA (**F**), and T-CHO (**G**) were measured in the mice (n = 6). Blood glucose levels were measured during a glucose tolerance test (**H**) and an insulin tolerance test (**J**). The area under the curve was plotted in (**I**) and (**K**), respectively. * denotes the level of statistical significance. ns no significance, $*p < 0.05$, $**p < 0.01$, $***p < 0.001$. Data are presented as mean ± SEM. Statistical analyses were performed using one-way ANOVA followed by Tukey's test (**C**–**G**, **I**, **K**).

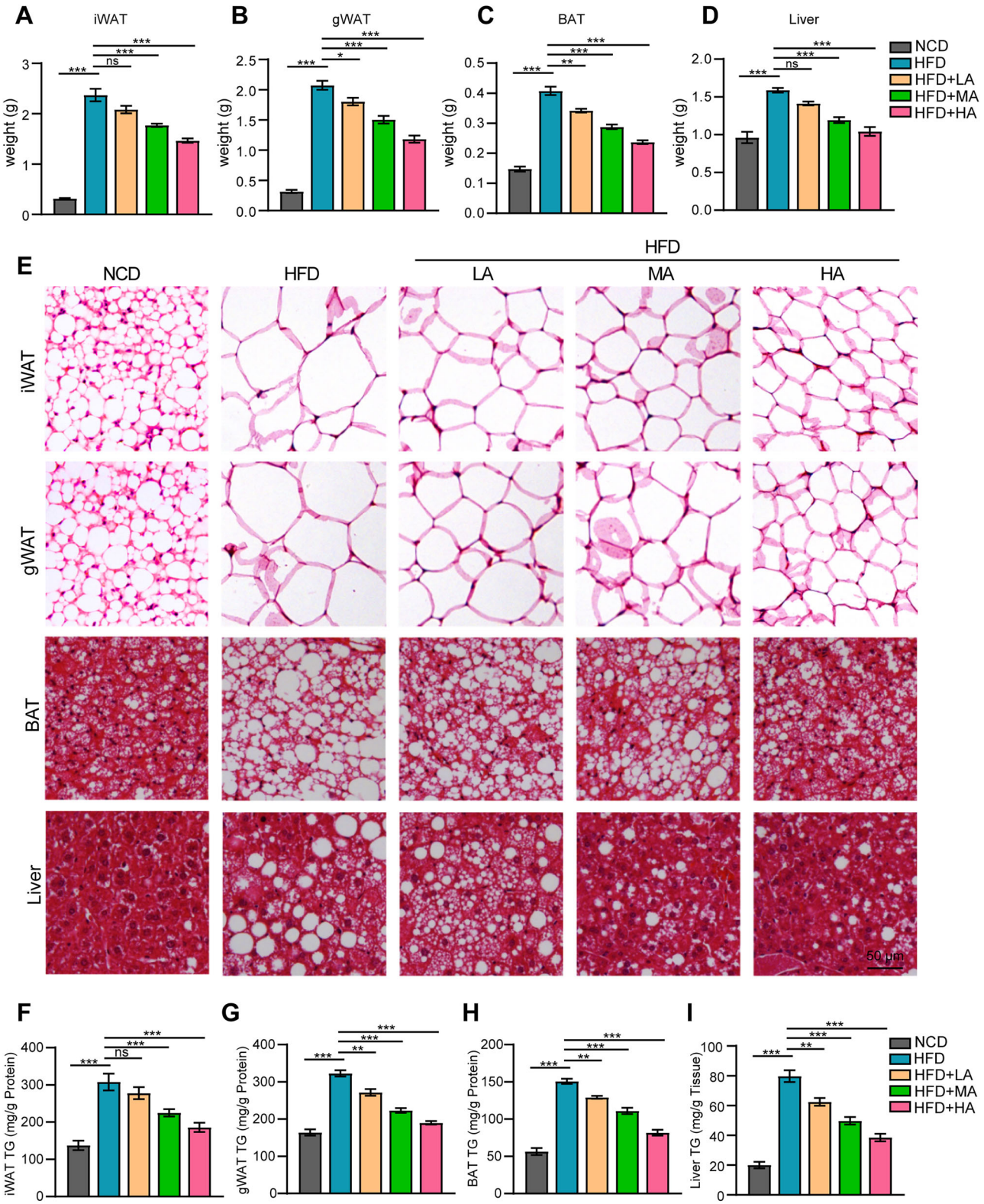

Fig. 2 | AAO significantly attenuates lipid accumulation in adipose tissue and the liver. Upon completion of the feeding regimen, mice were euthanized, and tissues from iWAT (**A**), gWAT (**B**), BAT (**C**), and liver (**D**) were harvested and weighed (n = 6). **E** Representative H&E staining of BAT, iWAT, gWAT and liver from mice. Scale bar, 50 μm. At week 12, the mice from each experimental group were euthanized, and the TAG levels in different tissues, including iWAT (**F**), gWAT (**G**), BAT (**H**), and liver (**I**), were quantified (n = 6). * denote the level of statistical significance. ns no significance, $^{**}p < 0.01$, $^{***}p < 0.001$. Data are presented as mean ± SEM. Statistical analyses were performed using one-way ANOVA followed by Tukey's test (**A**–**D**, **F**–**I**).

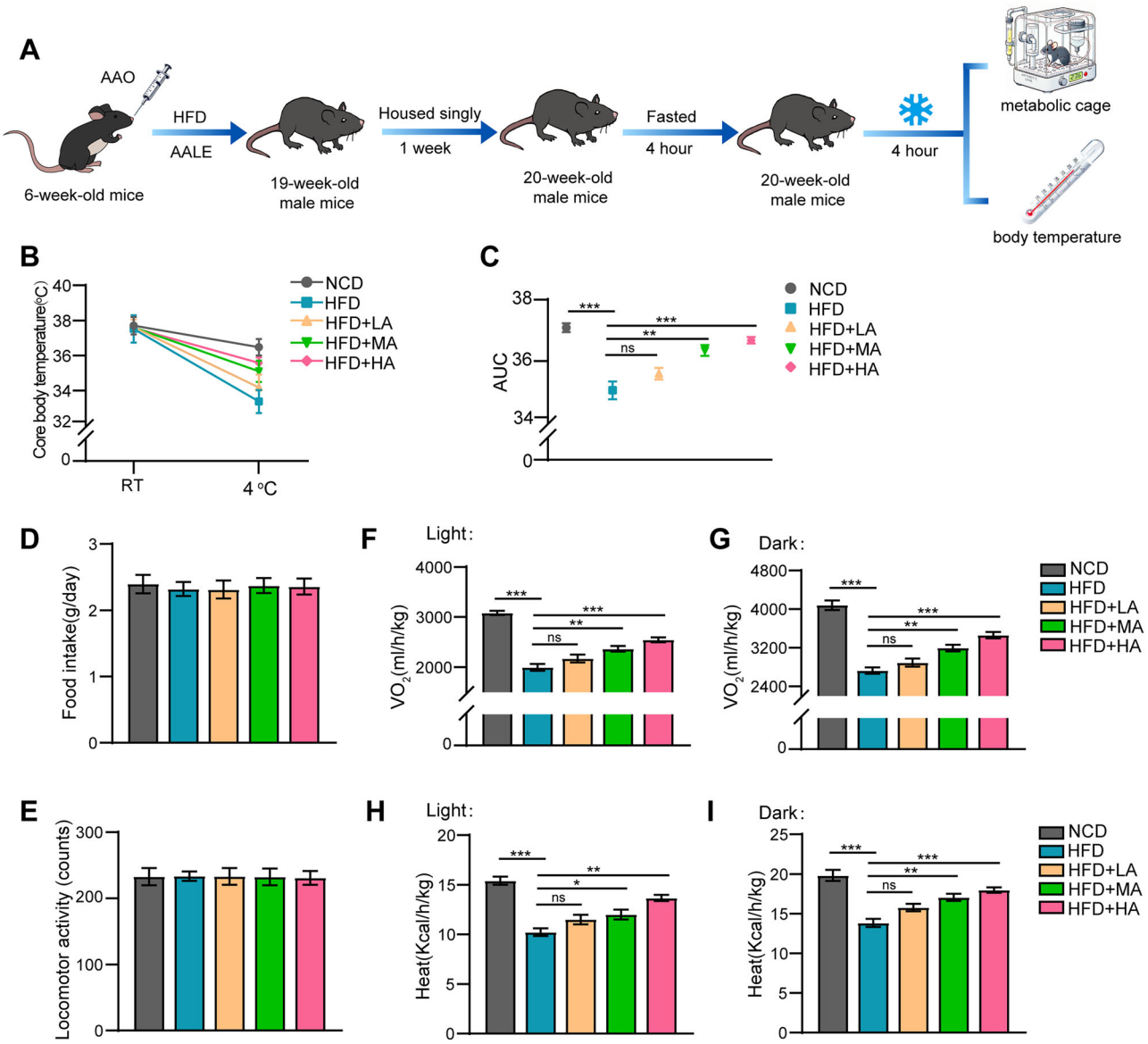

Fig. 3 | AAO significantly facilitates thermogenesis of mice. A Schematic diagram of the experimental design for cold tolerance and metabolic cage analysis. **B**, **C** The body temperature of mice from different groups under room temperature and cold exposure was measured (n = 6). During the 12-week period, the mice were housed individually for 1 week prior to metabolic cage analysis. Data on food intake and physical activity are presented in (**D**) and (**E**). Oxygen consumption (**F**, **G**) and heat production (**H**, **I**) were measured during both the light and dark cycles (n = 6). * denote the level of statistical significance. ns no significance, $*p < 0.05$, $**p < 0.01$, $***p < 0.001$. Data are presented as mean ± SEM. Statistical analyses were performed using one-way ANOVA followed by Tukey's test (**C**, **F**–**I**).

AAO promotes thermogenic gene expression and increases oxygen consumption in vitro

To further explore the role of AAO in regulating thermogenic gene expression in BAT, we isolated BAT SVFs from the BAT and induced differentiation into mature brown adipocytes. The cells were harvested after treatment with AAO for subsequent experiments (Fig. 7A). We first evaluated the toxicity of AAO on BAT SVFs, and found that AAO did not affect the proliferation of these cells (Fig. S10). As shown in Fig. 7B, the TG content in the MA and HA groups was significantly lower than that in the control cells ($p < 0.05$), while the TG content in the LA group was comparable to that of the control group. Furthermore, after treatment with AAO, the expression levels of UCP1 and PRDM16 were significantly higher than those in the control group (Fig. 7C-E and S11A). In contrast, with increasing concentrations of AAO, the expression levels of AGT and PPARγ gradually decreased (Fig. 7C, F, G and S11B). Consistent with the increased thermogenic genes, treatment with AAO significantly increased the basal and maximum respiration rates of the cells (Fig. 7H–J). Taken together, AAO promoted the expression of thermogenic genes and increased the respiratory rate of the cells in vitro.

AAO attenuates metabolic dysregulation in mice serum

To systematically analyze the impact of AAO on the metabolic profile of mice under HFD, this part employed untargeted metabolomics to analyze serum samples from both the HFD group and the AAO intervention group (n = 8/group). A total of 220 metabolites were identified, including key metabolic categories such as lipids, amino acids, and their derivatives (Supplementary Table 1), detected in both positive and negative ion modes. OPLS-DA was used to build a metabolite-group association model, and the results showed a significant separation in the metabolite distribution between the AAO group and the HFD group (cross-validation ANOVA, p = 0.0324; Fig. S12A), indicating that AAO intervention could reshape the serum metabolic profile. Moreover, a permutation test validated the model's

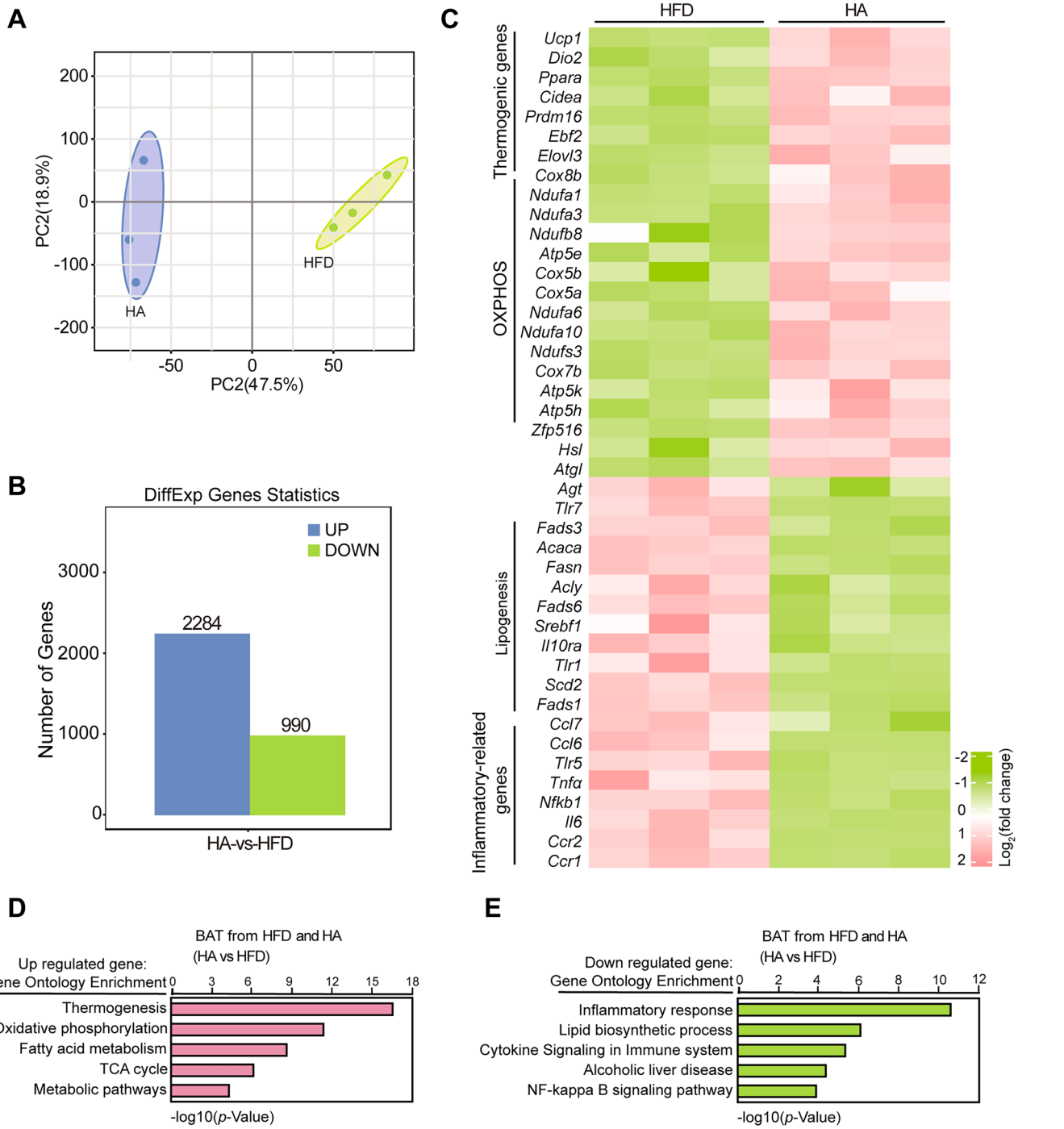

Fig. 4 | Impact of AAO on gene expression in BAT. RNA-seq analysis of BAT samples from mice in the HFD and HA groups. **A** Principal component analysis (PCA) of gene expression between the two groups of mice. **B** Quantification of upregulated and downregulated genes in the two groups of mice. **C** A heatmap was generated to illustrate the upregulated and downregulated differential genes between the HFD and HA groups. Functional enrichment analysis was performed on both the upregulated (**D**) and downregulated genes (**E**).

reliability (Fig. S12B), and principal component analysis (PCA) confirmed the metabolic differences between the two groups (Fig. 8A).

Differential metabolite analysis identified 22 metabolites with significant changes, of which 16 were upregulated in the HFD group, including lipid synthesis-related metabolites such as long-chain fatty acids and their derivatives, as well as inflammation-related metabolites such as aromatic amino acid metabolites (Fig. 8B). Conversely, 6 metabolites were downregulated in the HFD group, primarily involving intermediate products of energy metabolism (Fig. 8B). Notably, after AAO intervention, the expression of HFD-induced upregulated metabolites, such as long-chain fatty acids, was significantly reduced, while some downregulated metabolites, such as branched-chain amino acid metabolites, showed a trend toward restoration (Fig. 8B). This pattern suggests that AAO may alleviate HFD-induced metabolic disturbances by inhibiting lipid synthesis pathways and regulating amino acid metabolism. KEGG pathway enrichment analysis further revealed that the differential metabolites were predominantly enriched in the "biosynthesis of unsaturated fatty acids" and "biosynthesis of phenylalanine, tyrosine, and tryptophan" pathways (Fig. 8C). The regulation of lipid metabolites such as linoleic acid and palmitic acid, as well as tryptophan-derived compounds such as serotonin and indole-3-lactic acid,

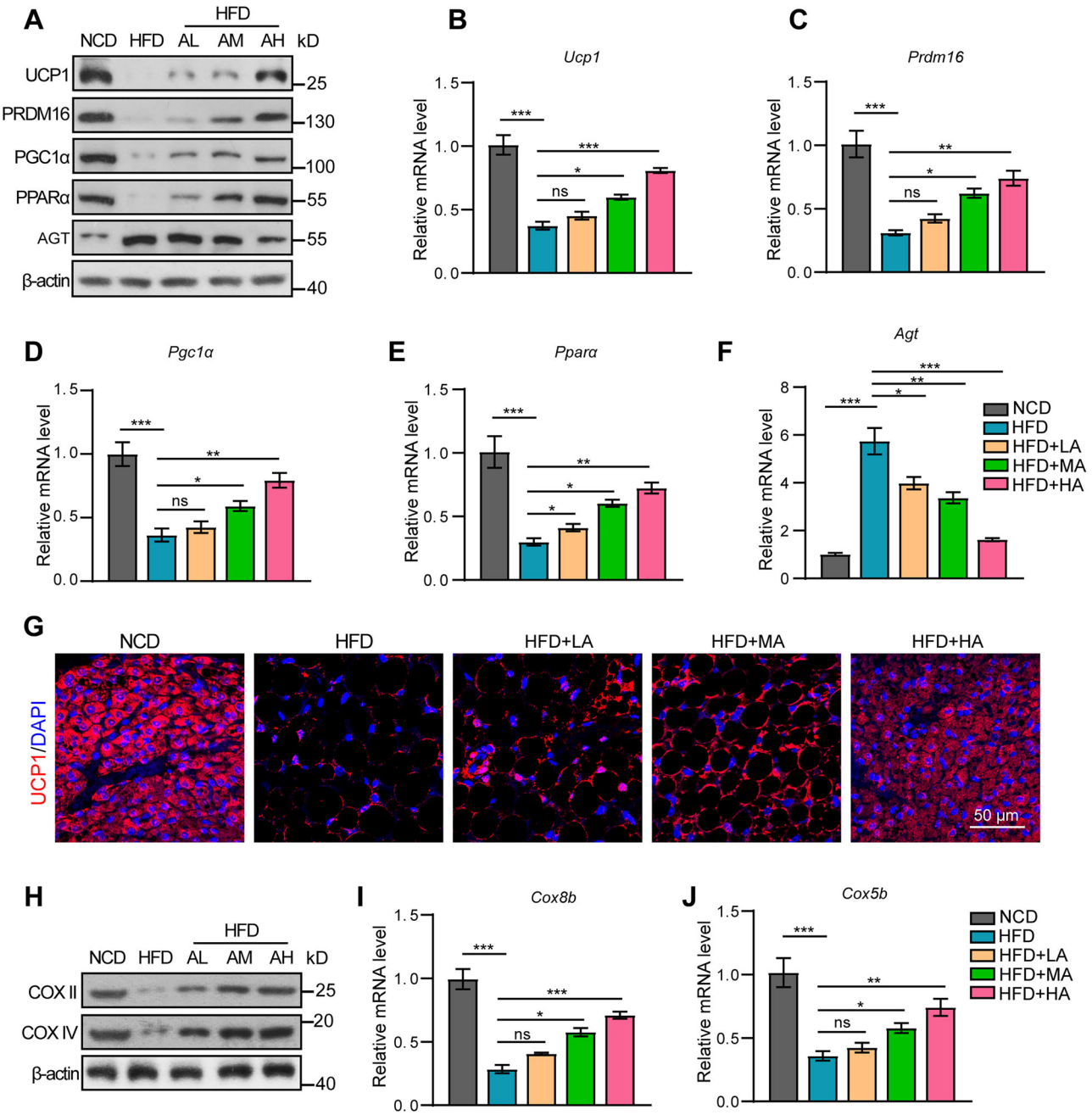

Fig. 5 | AAO enhances the expression of thermogenic and oxidative phosphorylation genes in BAT in vivo. A Western blot analysis showing the expression of UCP1, PGC1α, PPARα, PRDM16, and AGT in the BAT of mice from the NCD, HFD, LA, MA, and HA groups. **B**–**F** The mRNA levels of *Ucp1*, *Pgc1α*, *Pparα*, *Prdm16*, and *Agt* in the BAT of mice (n = 6). **G** Immunofluorescence (IF) analysis for the UCP1 expression in BAT of mice. Scale bar, 50 μm. **H** Protein expression levels of COXII and COXIV in BAT of mice. The mRNA levels of *Cox8b* (**I**) and *Cox5b* (**J**) in BAT were determined by qPCR analysis. * denote the level of statistical significance. ns no significance, $*p < 0.05$, $**p < 0.01$, $***p < 0.001$. Data are presented as mean ± SEM. Statistical analyses were performed using one-way ANOVA followed by Tukey's test (**B**–**F**, **I**–**J**).

may be closely related to the phenotypic improvements of AAO in alleviating fatty liver, suppressing inflammation, and enhancing insulin sensitivity (Fig. 8D–L). Thus, the results confirm that AAO can alleviate metabolic dysregulation in the serum of mice.

AAO promotes the expression of thermogenic genes by enhancing the expression of ZFP516

Prior research has indicated that cold exposure induces brown fat remodeling and enhances thermogenic capacity in both mice and humans[35,36]. We first compared RNA-seq data from HFD-HA BAT (Up-HFD-HA vs. HFD) with data from cold-exposed BAT (Up-4 °C vs. RT, GSE162907). Among the differentially expressed genes, 1183 were found to overlap, including *Zfp516*, *Ucp1*, and *Dio2* (Fig. S13). In parallel, we performed an RNA-seq data analysis, which revealed that ZFP516 expression was significantly elevated in the BAT of the HA group compared to the HFD group (Fig. 4C). As expected, genes upregulated by ZFP516 overexpression and those upregulated by oral AAO treatment were both enriched in thermogenic pathways in mice (Fig. 4D)[17].

Additionally, mice overexpressing ZFP516 exhibited elevated oxygen consumption and improved resistance to obesity, a phenotype that mirrors that observed in AAO-treated mice[17]. Therefore, we hypothesize that AAO promotes thermogenic gene expression in BAT through ZFP516.

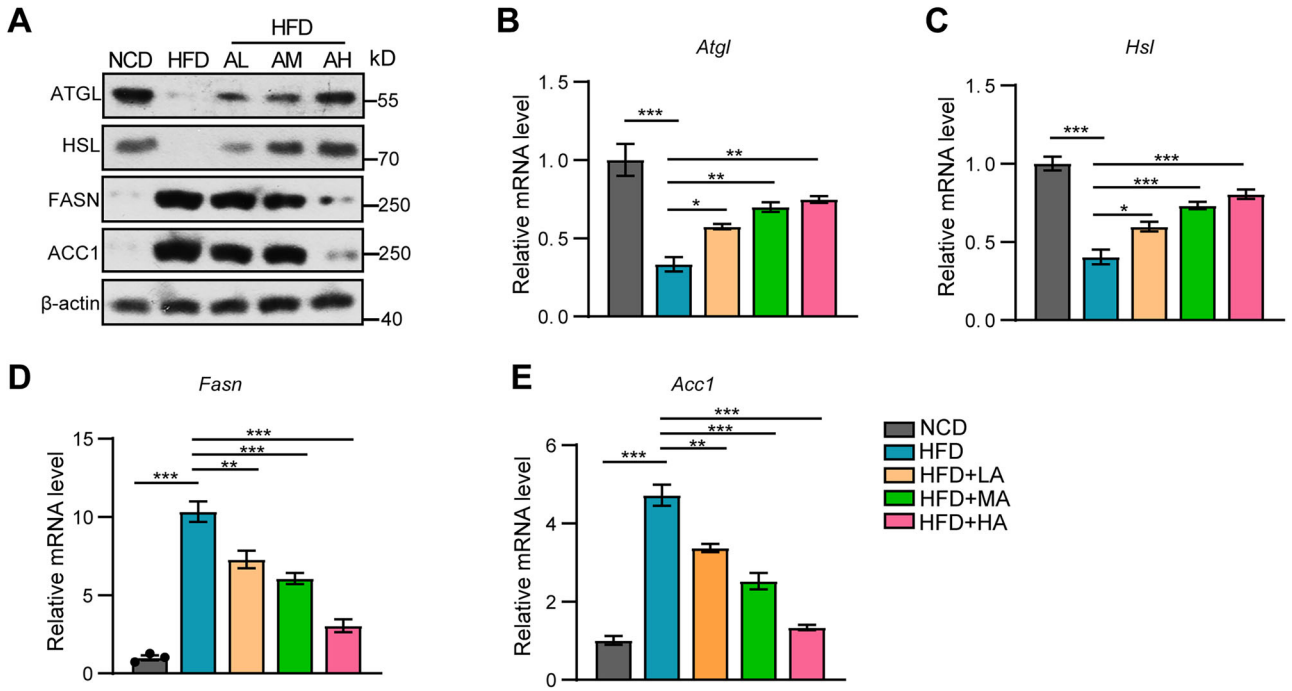

Fig. 6 | AAO upregulates lipolysis-related genes and downregulates genes associated with lipogenesis in BAT in vivo. A Protein expression levels of ATGL, HSL, FASN, and ACC1 in the BAT from each group mice. **B**–**E** The mRNA expression levels of *Atgl*, *Hsl*, *Fasn*, and *Acc1* in the BAT (n = 6). * denote the level of statistical significance. ns no significance, $^{*}p < 0.05$, $^{**}p < 0.01$, $^{***}p < 0.001$. Data are presented as mean ± SEM. Statistical analyses were performed using one-way ANOVA followed by Tukey's test (**B**–**E**).

Compared to the HFD group, the expression level of ZFP516 gradually increased with the rising concentration of AAO, while LSD1 expression remained unchanged by AAO (Fig. 9A, B and S14A). We performed a Venn analysis between the genes regulated by ZFP516 in ChIP-seq and those upregulated after AAO treatment, revealing that *Ucp1* is present in the intersection (Fig. 9C). As demonstrated in Fig. 9D, ZFP516 specifically interacted with the -1 kb promoter region of *Ucp1*, and its binding strength was markedly enhanced following treatment with the AAO. To further confirm whether AAO promotes the binding of ZFP516 to the promoter of *Ucp1*, we conducted ChIP assays. As shown in Fig. 9E, the binding of ZFP516 to the promoter of *Ucp1* increased with the higher concentration of AAO. Additionally, the -1 kb *Ucp1* promoter was found to be occupied by ZFP516 and H3K27ac in BAT, followed by a FAIRE-qPCR assay (Fig. 9D). As demonstrated in Fig. 9F, AAO effectively enhanced the accessibility of the promoter of *Ucp1* to ZFP516. LUC assays further demonstrated that AAO could promote ZFP516-mediated activation of Ucp1 (Fig. 9G). To investigate whether the activation of thermogenic genes by AAO relies on ZFP516, we constructed a cell line with ZFP516 knockdown in BAT SVFs (Figs. 9H and S14B). As shown in Fig. 9I, ZFP516 knockdown completely inhibited the activation of *Ucp1* by AAO. Analysis of protein-protein interactions using the STRING database (version 12.0) revealed that ZFP516 interacts with LSD1 (Fig. 9J). Interestingly, we found that AAO promoted the interaction between ZFP516 and LSD1, further enhancing the transcriptional activation of Ucp1 by the ZFP516-LSD1 complex (Fig. 9K–M). In summary, AAO promotes the expression of thermogenic genes in BAT through ZFP516.

Discussion

Obesity is strongly associated with diseases like type II diabetes, hypertension, cardiovascular issues, cancers, osteoarthritis, and fatty liver, and enhancing thermogenesis of BAT activity is crucial for the treatment of obesity[37,38]. In our study, AAO was extracted from *Artemisia argyi* leaves via hydrodistillation using a clevenger apparatus, with its chemical composition rigorously identified by GC-MS, ensuring batch consistency and providing a chemical basis for subsequent experiments. AAO administration significantly reduced body weight gain, fat mass, and serum levels of TG, NEFA, and T-CHO in HFD-fed mice. Moreover, AAO improved glucose tolerance and insulin sensitivity, indicating their beneficial effects on overall metabolic health. This is consistent with previous studies showing that AAO possess antioxidant, anti-inflammatory, and hepatoprotective properties, which may contribute to their anti-obesity effects by improving metabolic homeostasis[21,39]. These findings suggest that AAO could serve as an effective functional food for combating obesity. However, it is important to note that AAO exhibits significant chemical variability, with both its composition and concentration being influenced by genetic factors and environmental variables such as climate, soil, harvest season, and processing methods[40]. Consequently, future studies should systematically investigate the compositional differences in AAO derived from different regions, seasons, and processing techniques. This will help establish standardized protocols based on the "source—process—dosage" framework, ensuring the reproducibility, comparability, and clinical translation potential of its anti-obesity effects.

Notably, we found no significant differences in cold tolerance, heat production, or oxygen consumption in mice administered a 100 mg/kg dose of AAO (LA group) compared to the control group. We hypothesize that this lack of effect is due to the inability of the low AAO dose to sufficiently upregulate ZFP516 expression, thereby failing to activate downstream thermogenic genes regulated by ZFP516. Consistent with this hypothesis, thermogenic genes in the BAT of the LA group, including *Ucp1*, *Pgc1α*, and *Prdm16*, showed no significant differences relative to the control group. At the 200 mg/kg dose, a more pronounced effect was observed, with reductions in body weight, body fat percentage, serum T-CHO levels, and BAT mass, as well as significant improvements in cold tolerance, oxygen consumption. Furthermore, at doses exceeding 200 mg/kg, cold tolerance, oxygen consumption, and heat production continued to increase with rising AAO concentrations. At these higher doses, ZFP516 expression was significantly upregulated, suggesting that ZFP516 may directly promote the expression of thermogenic genes such as Ucp1 and Pgc1α, and recruit LSD1 to form a transcriptional complex that further enhances thermogenesis. Therefore, we hypothesize that the pharmacological threshold for AAO lies

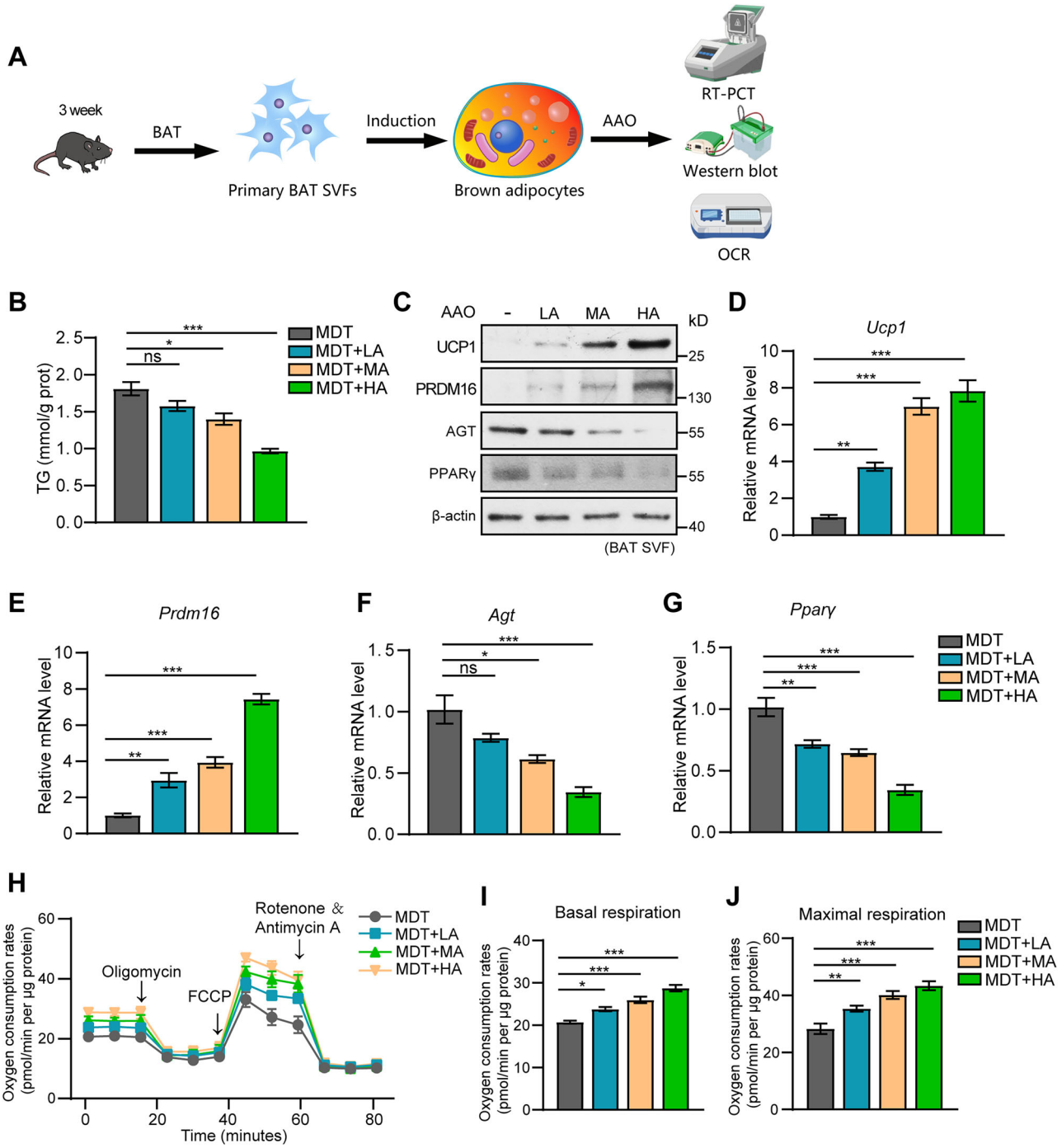

Fig. 7 | AAO enhances the expression of thermogenic genes and increases oxygen consumption in vitro. A The diagram illustrates that the BAT SVFs were isolated and differentiated into mature brown adipocytes, followed by AAO treatment for western blot analysis, qPCR, and OCR analysis. **B** The TG content in the cells of each group. **C** The protein expression levels of UCP1, PRDM16, AGT, and PPARγ in the cells of each group. **D–G** The mRNA expression levels of *Ucp1*, *Prdm16*, *Agt*, and *Ppary*. **H–J** BAT SVF cells were differentiated into brown adipocytes, followed by treatment with AAO. Oligomycin, FCCP, and Rotenone/Antimycin were added at the specified time points, indicated by the arrows, and the OCR data are shown in (**H**). The average basal and maximal respiration rates are presented in (**I**) and (**J**). * denote the level of statistical significance. ns, no significance, $*p < 0.05$, $**p < 0.01$, $***p < 0.001$. Data are presented as mean ± SEM. Statistical analyses were performed using one-way ANOVA followed by Tukey's test (**B**, **D–G**, **I**, **J**).

between 100 and 200 mg/kg. Further investigation is needed to refine the oral dosing regimen of AAO, with the goal of narrowing the pharmacological threshold for optimal therapeutic efficacy. Defining the pharmacological threshold of AAO is essential for refining dosing strategies in clinical applications. These insights will not only optimize treatment costs but also improve therapeutic efficacy and reduce adverse effects, ultimately enhancing clinical outcomes.

In rodents and newborn humans, BAT is primarily distributed in the interscapular, cervical, axillary, and perirenal regions, where it plays a key role in maintaining body temperature through non-shivering thermogenesis[16,41]. In adult humans, BAT is mainly located in the supraclavicular and cervical regions, and metabolically active BAT is associated with a decline in body weight[12,42]. Consistent with humans, enhancing BAT thermogenesis effectively counteracts HFD-induced weight gain in mice[30].

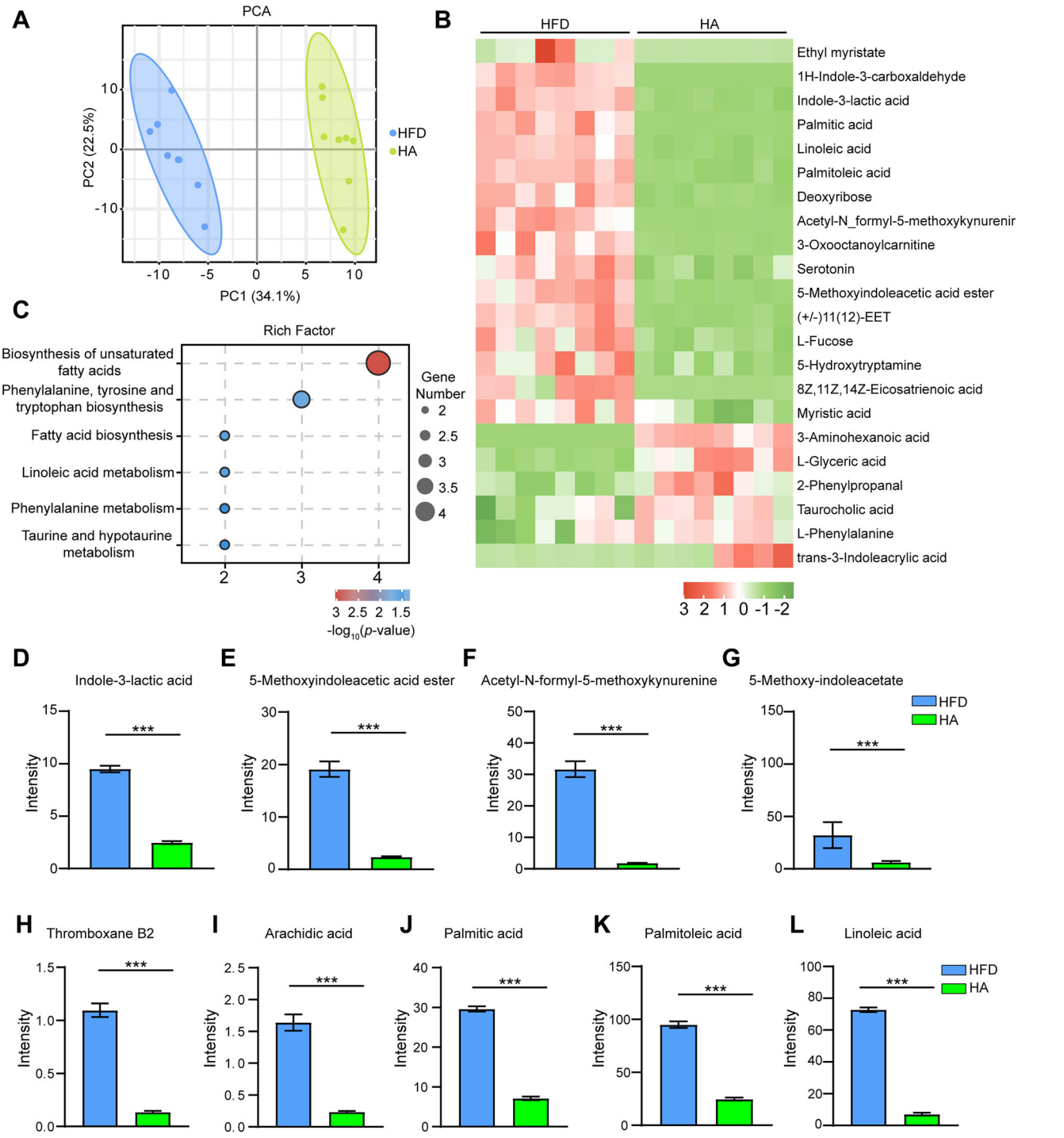

Fig. 8 | AAO attenuates metabolic dysregulation in mice serum. A PCA confirms significant metabolic differences between the HA and HFD groups. **B** Differential metabolite analysis identifies 23 metabolites with significant changes (n = 8). **C** KEGG pathway enrichment analysis. **D**–**L** The intensity of the specified metabolites detected by UPLC-HRMS. * denote the level of statistical significance, ***$p < 0.001$. Data are presented as mean ± SEM. Statistical analyses were determined by unpaired two-tailed Student's *t*test (**D**-**L**).

Our study demonstrates that AAO treatment enhances BAT thermogenesis in mice, increasing oxygen consumption and heat production, which contributes to its potential anti-obesity effects. Such evidence highlights the potential of enhancing BAT thermogenesis as a promising strategy for the treatment of obesity in humans. Additionally, AAO treatment significantly upregulated the expression levels of thermogenic genes, lipolysis-related genes, and mitochondrial oxidative phosphorylation genes. The increased expression of thermogenic genes, lipolysis-related genes, and oxidative phosphorylation genes, along with the decreased expression of lipogenic genes, led to enhanced energy expenditure and reduced lipid accumulation. The primary function of BAT is to counteract cold and obesity through non-shivering thermogenesis by oxidizing NEFA and glucose to generate heat[43,44]. AAO enhances lipolysis, promoting the release of NEFA, which is subsequently consumed by BAT, thereby reducing lipid accumulation. Simultaneously, AAO improves glucose tolerance in mice, enabling brown adipocytes to utilize glucose more efficiently and enhance the thermogenic

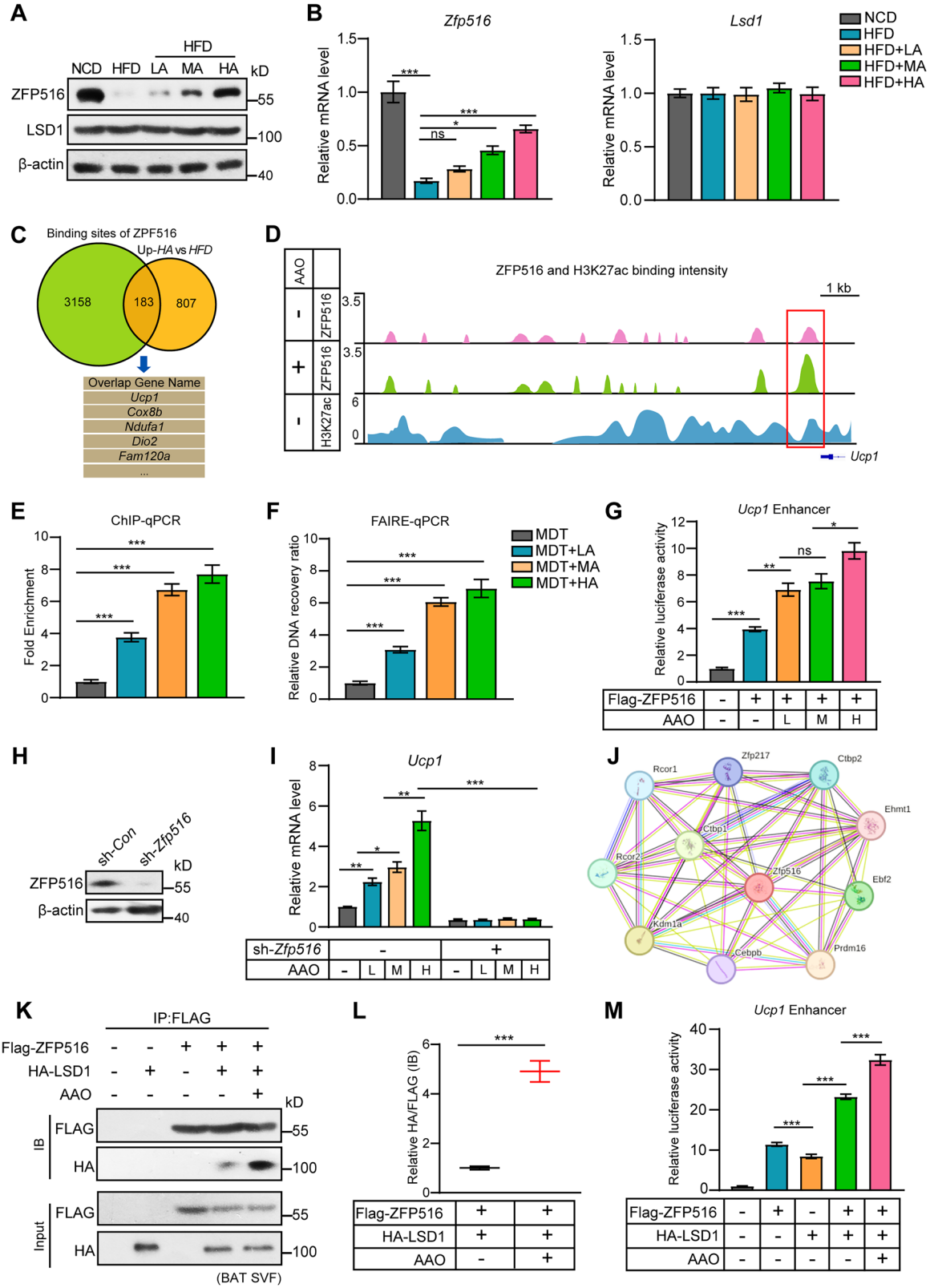

function of BAT. Therefore, AAO may exert anti-obesity effects by promoting BAT thermogenesis, aligning with the increasing demand for plant-based ingredients that support energy balance and healthy weight management.

Additionally, serum metabolomics analysis revealed that AAO significantly reduced the levels of linoleic acid, palmitic acid, and tryptophan metabolites. This suggests that AAO helps improve metabolic disorders by inhibiting lipid synthesis pathways and modulating tryptophan metabolism. These systemic metabolic alterations align with the upregulation of lipolytic genes and the downregulation of inflammatory factors in BAT, further reinforcing the anti-obesity mechanism of AAO through their multi-target regulation of the energy metabolism network.

Fig. 9 | AAO promotes the expression of thermogenic genes through ZFP516 in BAT. Western blot (**A**) and qPCR (**B**) analysis of ZFP516 and LSD1 expression levels in BAT from the NCD, HFD, LA, MA, and HA groups (n = 6). **C** Venn diagram showing the intersection between genes regulated by ZFP516 in ChIP assays and those upregulated by AAO treatment, with UCP1 identified as a common gene. **D** We reanalyzed our ChIP-seq data along with the ChIP-seq results from the GSE144188 database to examine the binding profiles of ZFP516 and H3K27ac on the promoter of *Ucp1*. **E** ChIP assays reveal that the binding of ZFP516 to the UCP1 promoter is enhanced with increasing concentrations of AAO. **F** The chromatin accessibility of mature brown adipocytes after AAO treatment was assessed by FAIRE-qPCR. **G** The luciferase assay was used to assess the activation of the *Ucp1* promoter in mature brown adipocytes after different treatments. (**H**) The protein levels of ZFP516 in Zfp516 knockdown cells and control cells. **I** ZFP516 knockdown in BAT SVF cells completely inhibited the activation of *Ucp1* expression in response to AAO treatment. **J** Protein interaction analysis with ZFP516 was performed using the STRING database (version 12.0). **K–M** HEK293T cells were transfected with Flag-ZFP516 and HA-LSD1 constructs. Forty-eight hours post-transfection, cells were collected and subjected to IP using anti-Flag beads. The input and precipitated fractions were subsequently analyzed by western blotting with the specified antibodies (**K**,**L**). Transcriptional activity of the -1 kb region of the *Ucp1* reporter under different treatments (**M**). * denote the level of statistical significance. ns, no significance, $^{*}p < 0.05$, $^{**}p < 0.01$, $^{***}p < 0.001$. Data are presented as mean ± SEM. Statistical analyses were performed using one-way ANOVA followed by Tukey's test (**B**, **E**-**G**, **M**), two-way ANOVA followed by Tukey's test (**I**), and unpaired two-tailed Student's *t* test (**L**).

Previous research has demonstrated that only acute cold stimulation can increase the expression of ZFP516, after which ZFP516 recruits LSD1 to the Ucp1 promoter, thereby enhancing the thermogenic function of BAT[17,18]. Promoting the expression of ZFP516 and activating the ZFP516-LSD1 complex are crucial for maintaining energy homeostasis and combating obesity[18]. However, no studies have reported that any major constituent of the oil or other related natural compounds are known to promote the expression of ZFP516 and activate the ZFP516–LSD1 complex. In our study, we present the novel finding that AAO, as a natural extract, promotes the expression of ZFP516 and enhances the activity of the ZFP516–LSD1 complex. The activation plays a critical role in promoting the thermogenic capacity of BAT, marking the first report of a natural compound capable of modulating this complex. Previous studies have shown that capsaicin, by activating the TRPV1 receptor, increases energy expenditure and promotes thermogenesis, potentially aiding in weight regulation and combating obesity[45]. In addition to activating the ZFP516-LSD1 complex, AAO also significantly enhances the expression of PPARα, a key regulator of lipid metabolism and energy homeostasis[46]. We hypothesize that AAO may also stimulate thermogenesis in BAT through the activation of PPARα. Combining AAO with capsaicin may enhance its metabolic benefits, offering a novel strategy for combating obesity through dietary intervention. Therefore, as a functional food and natural activator, AAO effectively targets the ZFP516-LSD1 pathway, presenting a novel mechanism for its potent anti-obesity effects.

Artemisia argyi extract (60 mg) exhibits significant efficacy in the clinical treatment of acute and chronic gastritis. It effectively improves gastric mucosal erosion, promotes the healing of erosions, alleviates hemorrhagic lesions, and relieves gastrointestinal symptoms. Furthermore, *Artemisia argyi* extract demonstrates good safety, with no severe adverse events or drug reactions observed, and patients show good tolerance to the treatment[23]. Our study highlights the potential of AAO as a novel functional lipid component in metabolism-oriented food formulations. GLP-1 receptor agonizts like semaglutide and liraglutide effectively control blood glucose and reduce body weight through enhanced insulin secretion and appetite suppression, but are associated with notable renal, gastrointestinal, and pancreatic side effects[47]. Derived from a traditional plant, AAO may have fewer side effects compared to synthetic drugs and could potentially be used safely and effectively as a dietary supplement or functional food in humans in the future. However, further studies are required to determine the effective dosage of AAO for obese patients and to establish its bioavailability, safety, and efficacy in humans. Additionally, the use of male mice exclusively may limit the representativeness and generalizability of our findings. Future studies should incorporate female mice to improve the broader applicability of the conclusions. Meanwhile, future research should investigate the potential synergies between AAO and other bioactive compounds, such as dietary fibers or probiotics, to develop multi-functional food products for obesity prevention. Finally, the mechanisms underlying the effects of AAO on other metabolic tissues, such as white adipose tissue and liver, should be investigated to provide a comprehensive understanding of their anti-obesity actions.

Methods

AAO extraction

The *Artemisia argyi* leaves, obtained from a local market in Xiamen, Fujian, were ground and subjected to hydrodistillation using a Clevenger apparatus to extract AAO. The leaves were distilled overnight, and the essential oil was dried with anhydrous sodium sulfate, aliquoted, sealed, and stored under refrigerated, light-protected conditions. To ensure consistency, only one batch of AAO was used in the animal experiments. The essential oil samples were analyzed by GC-MS using a TR-5MS capillary column in electron impact ionization mode (70 eV). The mass spectra were recorded in full-scan mode (m/z 40–500) with helium as the carrier gas at 1.0 mL/min. A 2 μL split injection was performed with a 1:10 split ratio. The temperature program was as follows: 60 °C for 2 min, ramped to 170 °C at 5 °C/min, held for 2 min, then ramped to 250 °C at 20 °C/min and held for 2 min. Volatile compound identities were confirmed by comparing the spectra with databases.

Animal experiment design

Mice were group-housed at a density of five per cage under controlled environmental conditions, with a temperature range of 22–24 °C, relative humidity maintained at 50–60%, and a 12-h light/dark cycle beginning at 07:30. In this study, we selected male mice due to their stable hormone levels, higher thermogenic capacity, and extensive precedent in BAT research, ensuring the reproducibility and stability of the results[48,49]. Male C57BL/6 mice, age-matched for each experiment, were obtained from the Shanghai Model Organisms Center or GemPharmatech. The high-fat diet was supplied by Readydietech Co., Ltd. (Shenzhen, China), and the standard chow diet by Jiangsu Xietong Pharmaceutical Bio-engineering Co., Ltd. Mice were divided into five groups: normal chow diet (NCD), high-fat diet (HFD), and high-fat diet with oral AAO at low (LA), medium (MA), or high (HA) concentrations, with 10 mice in each group. The HFD group had unrestricted access to the high-fat diet, while the LA, MA, and HA groups received 100 mg/kg, 250 mg/kg, or 400 mg/kg of AAO. At the end of the experiment, the mice were briefly anesthetized with 3–4% isoflurane and then euthanized by gradual-fill CO_2 asphyxiation (30–70% chamber volume per minute). Death was confirmed by the absence of cardiac and respiratory activity for ≥2 min. Subsequently, intrascapular BAT, WAT, and liver tissue of mice were immediately collected for further experiments. All animal experiments were approved by the Institutional Animal Care and Research Advisory Committee of Xiamen University (Permit No. XMULAC20230105).

Pharmacokinetic and toxicological experiment

For the pharmacokinetic experiment, male Sprague–Dawley rats (weight 210 ± 15 g, n = 4 per group) were orally administered AAO at a dose of 500 mg/kg. Blood samples (approximately 600 μL) were collected at 0, 0.5, 1, 2, 4, and 8 h, and plasma was separated. The concentration of cineole was quantified using gas chromatography-flame ionization detection (GC-FID), with cyclohexanone as the internal standard. Pharmacokinetic parameters were calculated using a non-compartmental model and analyzed with DAS 3.0 software.

For the toxicity experiment, 8-week-old male mice were orally administered AAO at doses of 100, 250, or 400 mg/kg once a week. At the age of 30 weeks, blood samples were collected to measure ALT, AST, ALP (Jiangsu Meimian Industrial Co., Ltd), BUN, creatinine, cTnT (LANSO, Cat#-AE92646Mu), cTnI, and BNP levels (Shanghai Jinma Laboratory Equipment Co., LTD). Then, the locomotor activity of the mice was monitored using a metabolic cage system. At the end of the experiment, mice were then euthanized, and skeletal muscle tissues were collected for histopathological examination using H&E staining kit.

Body-composition analysis and metabolic cage analysis

The mice were immobilized in a designated container, and their fat and lean mass were assessed using the composition analyzer (SUZHOU NIUMAG Co., Ltd, Cat#QMR06-060H-PRO). Mice were individually housed at 22 °C for 1 week, followed by a 2-day acclimatization in metabolic cages. The Sable Promethion system was used to measure food intake, body weight, oxygen consumption, heat production, and locomotor activity.

Glucose tolerance tests and insulin tolerance tests

For the glucose tolerance test (GTT), mice were fasted for 16 h and injected intraperitoneally with 1.0 g/kg D-glucose. In the insulin tolerance test (ITT), mice were fasted for 6 h, then injected with 1.5 U/kg human insulin (TargetMol, USA, Cat#T8221). Blood samples were collected from the tail vein at the indicated time points post-injection to measure blood glucose levels using a glucometer.

Serum analysis

Before euthanasia, blood was collected from the mice's eyeballs and allowed to clot at 4 °C for 4–6 h. The samples were then centrifuged at 1, 500 g for 10 min at 4 °C (DLAB Scientific Co., Ltd, Cat#DM0436E), and the supernatants were transferred to new tubes (LABLEAD Inc, Cat#LXG0150). TG, T-CHO, NEFA, ALT, and AST levels were measured using corresponding assay kits (Nanjing Jiancheng Bioengineering Institute for TG, T-CHO, ALT, and ALT; Bioswamp, Cat#BTK026 for NEFA), following the manufacturer's instructions.

Immunohistochemistry and immunofluorescence

For H&E staining, indicated tissues were collected and fixed in 4% paraformaldehyde (PFA) at room temperature (RT) for 12 h. After fixation, the tissues were dehydrated through an ethanol gradient, embedded in paraffin, and sectioned into 3 μm thick slices. The tissue sections were then stained using the H&E staining Kit (Wanleibio, Cat#WLA051a; Solarbio, Cat#G1106) following the manufacturer's instructions.

For immunofluorescence, antigen retrieval was performed using an antigen retrieval solution (Keygen BioTECH, Cat# KGC3110). The slides were blocked with 2.5% Fetal Bovine Serum (FBS) (EXCellBio, Cat#FSP500) and 0.15% Triton X-100 (HUAYUN, Cat#SHB50396) in PBS (Pricella, Cat#PB180327) for 1.5 h. The slides were then incubated with primary antibodies: anti-UCP1 (Abclonal, Cat#A5857) (dilution 1:100). Afterward, the sections were incubated with secondary antibodies conjugated to fluorescent dyes (Elabscience, Cat#E-IR-R119) for 1 h at RT in the dark. To stain the nuclei, the slides were treated with 5 μg/ml DAPI (Mei5 Biotech, Cat#MF681-plus-01) for 10 min. Imaging was carried out using a Zeiss LSM 780 confocal microscope.

Serum Non-targeted Metabolomics

A 100 μL serum sample was mixed with 400 μL pre-chilled extraction solution (methanol: acetonitrile: water = 2:2:1) and magnetic beads, then incubated at −20 °C for 1 h to precipitate proteins. After centrifugation, the supernatant was dried under vacuum. For reconstitution, 200 μL of acetonitrile and 200 μL of water were added, followed by centrifugation and filtration through a 0.22 μm filter (Schbio Biotechnology). Metabolite detection was performed using a Dionex UltiMate 3000 UHPLC system coupled with a Q Exactive mass spectrometer, with Waters ACQUITY UPLC HSS T3 column and a 15-min gradient elution. Positive and negative ion detection were carried out using specific mobile phases, and 2 μL of sample was injected. Data were processed with Compound Discovery 3.3 software.

qPCR analysis and RNA-seq analysis

For qPCR analysis, total RNA was extracted from samples using TRIzol reagent (Accurate Biology, Cat#AG21101) and isopropanol (Shanghai Acmec Biochemical Technology Co., Ltd). For cDNA synthesis, a cDNA synthesis kit (Abm, Cat#G592) was used, and reactions were carried out in PCR tubes (Jet Biofil, Cat#PCR411200). Gene expression levels were quantified using a real-time PCR system (Roche) with SYBR Green (Yeasen, Cat#11201ES08). To normalize the data, 18S mRNA was used as the internal control. The primer sequences employed for qPCR are listed in Supplementary Table 2.

For RNA-Seq analysis, total RNA was extracted from samples using an RNA Extraction Kit (Boxbio, Cat#AKNA001-1). RNA-Seq libraries were constructed from 1 μg of RNA via poly (A) selection, cDNA synthesis, adapter ligation, and amplification (YoungGen, Cat#RM103A). Sequencing was performed using the Illumina HiSeq2500 platform, and subsequent data analysis was conducted by Gene Denovo Biotechnology Co. (Guangzhou, China).

Western blot analysis

Samples were lysed using RIPA buffer (APExBIO, Cat#K1120, Houston, USA) supplemented with phosphatase and protease inhibitors (TargetMol), and sonicated with an ultrasonic processor (SCIENTZ). Protein concentrations were determined using a BCA protein assay kit (NCM Biotech, Cat#WB6501), and 40 μg of total protein was loaded per sample. The samples were separated by SDS-PAGE (CYTOCH, Cat#PW0002) in Tris-Glycine buffer (Boyi Biotech, China, Cat#BR0148-01). Membranes were blocked with Fastest Blocking Reagent (HYCEZMBIO, Cat#HYC00811) and incubated with primary antibodies at the following dilutions: UCP1 (Diagbio, Cat#db9840) (dilution 1:1000), PRDM16 (Santa, Cat#sc-517625) (dilution 1:1000), PGC1α (SAB, Cat#37818) (dilution 1:1000), β-actin (Sino Biological, Cat#109444-T36) (dilution 1:20000), FASN (BOSTER, Cat#PB9865) (dilution 1:1000), PPARα (Biodragon, Cat#BD-PB4080) (dilution 1:1000), HSL (ZENBIO, Cat#344379) (dilution 1:1000), Flag (Sigma-Aldrich, Cat#F7425) (dilution 1:1000), HA (Bioss, Cat#BMS0966M) (dilution 1:1000), PPARγ (Bioworld, Cat#BS79617) (dilution 1:1000), ATGL (Abways, Cat#CY8408) (dilution 1:1000), ACC1 (HABIO, Cat#ET1609-77) (dilution 1:1000), IL10 (Solarbio, Cat#K009382P) (dilution 1:1000), TNFα (ELK Biotechnology, Cat#EA251) (dilution 1:1000), ZFP516 (GenScript) (dilution 1:1000), and LSD1 (PTM BIO, Cat#PTM-5960) (dilution 1:1000). After incubation with HRP-Goat Anti-Mouse Recombinant Secondary Antibody (Shanghai Epizyme, Cat#LF101) (dilution 1:5000) and HRP-Goat Anti-Rabbit IgG Antibody (GenScript, Cat#A00098) (dilution 1:5000), protein signals were visualized using enhanced chemiluminescence (Abbkine, Cat#BMU101).

Plasmids, lentivirus packaging and infection

For lentiviral overexpression plasmid construction, mouse Zfp516 and Lsd1 were amplified from a cDNA library derived from mouse BAT and purified using the Fast PCR and Gel DNA Purification Kit (YALI Biotech, Cat#YC48001-200). The purified fragments were then inserted into the pLV-N-Flag/HA-XM vector using T4 DNA ligase (CUSABIO, Cat#CSB-YP355583EDZ, https://www.cusabio.com). For knockdown experiments, the corresponding shRNAs were cloned into the pLKO.1 plasmid. The plasmid was amplified in Stbl3 competent cells (Coolaber, Cat#CC518) and subsequently extracted using a SPI-Neasy Plasmid Midiprep Kit (MP Biomedicals, Cat#116539025). Lentiviral particles were generated by transfecting the constructed plasmids into HEK293T cells, along with the pHR and pVSV-G plasmids, using EZ-Trans transfection reagent (Shanghai Life-iLab Biotech, Cat#AC04L092) according to standard protocols[50]. Lentivirus was collected and concentrated 48 h post-transfection (Cobetter, Cat#ULRC1000150P). For infection, cells were cultured to 75% confluence and infected with lentivirus in medium containing 10 μg/ml

polybrene (HUAYUN, Cat#HYP490). After 36 h, the infected cells were selected with 5 μg/ml puromycin for 1 week to establish stable cell lines.

Immunoprecipitation

The cells were lysed in IP buffer (AMEKO, Cat#RC62370) supplemented with protease and phosphatase inhibitors. The lysates were incubated with FLAG Magnetic Beads (Shanghai EpiZyme, Cat#YJ007) at 4 °C for 8 h. Afterward, the immunoprecipitated proteins were captured using a magnetic rack (QW-bio, Cat#666001) and analyzed by western blot using the indicated antibodies.

Luciferase reporter assays

The *Ucp1* promoter regions were amplified from mouse genomic DNA (Novoprotein, Cat#NR005) and inserted into the pGL4.26 plasmid to construct the luciferase reporter plasmid (Sevenbio, Cat#SM290). The resulting luciferase reporter plasmids, along with β-galactosidase and other specified plasmids, were transfected into cells using EZ-Trans transfection reagent (AbBOX, Cat#KX0110055). After 48 h of transfection, cells were collected for subsequent luciferase and β-galactosidase assays (Neobioscience, Cat#LAS106.10).

Cell culture

HEK293T (Pricella) cells were cultured in high-glucose DMEM (Cytiva, Cat#SH30285.01) supplemented with 1% non-essential amino acids (NEAA) (IMMOCELL, Cat#IMC-D07), 1 mM sodium pyruvate (Biochannel, Cat#BC-CE-027), 100 U/ml penicillin, 100 μg/ml streptomycin (BasalMedia Co., Ltd, Cat#S110JV), and 10% FBS (AMOBIO, Cat#FB-SAB001) at 37 °C in a 5% CO_2 atmosphere.

Brown stromal-vascular fraction cells (SVFs) were isolated from interscapular BAT using 3 mg/mL collagenase II (Sigma)[30]. The SVFs were cultured in high-glucose DMEM (SUNNCELL, Cat#SNM-002A), supplemented with 20% FBS (CellMax, Cat#SA201) at 37 °C in an 8.8% CO_2 atmosphere. When the cells reached 95% confluence in 6-Well Plate+6 Inserts, 1 μm Pore Size PET (Polyester) Membrane (Wuxi NEST Biotechnology Co., Ltd, Cat#723431), then they were treated with Medium A, containing 1 nM 3,3',5-Triiodo-L-thyronine (T3) (Sigma-Aldrich, Cat#T2877), 0.125 mM indomethacin (Sigma-Aldrich, Cat#I7378), 1 μM rosiglitazone (GLPBIO, Cat#GC16444), 5 μM dexamethasone (Sigma-Aldrich, Cat#D1756), 850 nM insulin (MCE, Cat#HY-P0035), and 0.5 mM 3-isobutyl-1-methylxanthine (IBMX) (Sigma-Aldrich, Cat#I5879) for 48 h. Subsequently, cells were cultured in Medium B, which contained 1 nM T3, 1 μM rosiglitazone, and 850 nM insulin, with medium changes every 2 days. On day 6, mature brown adipocytes were treated with AAO at concentrations of 10 μg/ml, 20 μg/ml, and 30 μg/ml, designated as low, medium, and high concentrations, respectively. After 16 h of treatment, the cells were harvested for further analysis.

Chromatin immunoprecipitation (ChIP) assay

Brown preadipocytes were infected with lentiviruses expressing pLV-Flag-empty or pLV-Flag-ZFP516 constructs. After infection, the cells were cultured to full confluence and differentiated into mature brown adipocytes in culture plates (CellPro Biotechnology, Cat#803006). The cells were fixed with 1% PFA at 37 °C for 15 min in a centrifuge tube (SAINING Biotechnology, Cat#3031111). The cells were then lysed using lysis buffer (MP Biomedicals, Cat#116544050) for 15 min on ice. The DNA of the cells was fragmented to a range of 200–800 base pairs using an ultrasonic processor (SCIENTZ, Cat#SCIENTZ08-IIIA). The supernatant was then incubated with FLAG Magnetic Beads (Biolinkedin, Cat#L-1011) overnight at 4 °C. The experiment was performed according to the provided manual instructions (GZSC Bio Co., Ltd, Cat#KT101). DNA enrichment was assessed by qPCR and normalized to the input sample (CWBIO, Cat#CW0957H). Primer sequences are listed in Supplementary Table 2.

Oxygen consumption rate (OCR) assay

Brown adipocytes were differentiated into mature brown adipocytes and seeded onto an XFe96 cell culture microplate. OCR was measured using the XF96 Extracellular Flux Analyzer according to the manufacturer's instructions. The culture medium was replaced with Seahorse XF DMEM (Eallbio, Beijing china; Cat#03.1001C), supplemented with 25 mM glucose (AoRuiCell Bio, Cat#ORCPB0418), 1 mM sodium pyruvate (Keygen Biotech, Cat#KGL2313-10), and 2 mM glutamine. During the OCR assay, sequential injections of 2 μM oligomycin (Shandong Sparkjade Biotechnology Co., Ltd, Cat#SJ-MA0524), 2.3 μM FCCP, and 1 μM rotenone/antimycin were added to measure uncoupled respiration, maximal respiration, and non-mitochondrial respiration, respectively. OCR data were normalized to protein content.

CCK8 assay

Cells were seeded in 96-well plates (Bioland, Cat#CCP06-096) at a density of 3500 cells per well and allowed to adhere for 12 h. Subsequently, the cells were treated with AAO at concentrations of 10 μg/ml, 20 μg/ml, and 30 μg/ml, referred to as low, medium, and high concentrations, respectively. Prior to each measurement, 10 μL of CCK-8 reagent (Biolight, Cat#CCK001) was added to each well, followed by incubation at 37 °C for 2 h. Absorbance was measured at 450 nm using a microplate reader (Bio-Rad). All experiments were conducted in triplicate.

Formaldehyde-assisted isolation of regulatory elements (FAIRE) assay

Cells were grown to 95% confluence and fixed with 1% PFA at room temperature for 10 min in centrifuge tubes (PakGent). After fixation, cells were lysed with SDS buffer on ice for 10 min. DNA was fragmented to 200–1000 base pairs by sonication under optimized conditions. The samples were centrifuged, and the supernatants were collected and treated with RNase A at 37 °C for 1 h. The samples were split into two portions: one for de-crosslinked DNA (control) and one for non-de-crosslinked DNA. For the de-crosslinked fraction, proteinase K (Macklin, Cat#P6321) was added, and incubation occurred at 37 °C for 8 h, followed by 6 h at 65 °C. Both fractions were purified using phenol-chloroform extraction. Chromatin accessibility was assessed by qPCR using primers listed in Supplementary Table 2, and data were analyzed using the FAIRE-PCR method.

Quantification and statistical analysis

Statistical analysis was performed using GraphPad Prism 8.0.2, with results expressed as mean ± SEM. Data normality was assessed using the Anderson-Darling, D'Agostino-Pearson, Shapiro-Wilk, or Kolmogorov-Smirnov tests, depending on the data type. For comparisons between two groups, an unpaired two-tailed Student's *t* test was used. For multiple group comparisons, one-way or two-way ANOVA followed by Tukey's test was applied, as indicated in the figure legends. Mouse age and sample sizes are also provided in the figure legends. Immunoblotting assays were analyzed using ImageJ software (National Institutes of Health). Statistical significance was considered at $^{*}p < 0.05$, $^{**}p < 0.01$, and $^{***}p < 0.001$, ns no significance. Experimenters were not blinded to group assignment during data collection.

Data availability

The datasets supporting this study are available as follows: RNA-Seq data: Gene Expression Omnibus GSE162907; ChIP-Seq data: Gene Expression Omnibus GSE144188. All data necessary to evaluate the conclusions of the paper are included within the manuscript and/or Supplementary Materials. Additional data related to this study can be requested from the corresponding author.

Code availability

The code used to support the results of this study is available from the corresponding author upon request.

Received: 28 May 2025; Accepted: 4 November 2025;
Published online: 13 December 2025

References

1. Raspa, M., Bailey, D. B., Bishop, E., Holiday, D. & Olmsted, M. Obesity, food selectivity, and physical activity in individuals with fragile X syndrome. *Am. J. Intellect. Dev. Disabil.* **115**, 482–495 (2010).
2. Maitin-Shepard, M. et al. Food, nutrition, and autism: from soil to fork. *Am. J. Clin. Nutr.* **120**, 240–256 (2024).
3. Liu, C. et al. Global health impacts of high BMI: a 30-year analysis of trends and disparities across regions and demographics. *Diab. Res. Clin. Pract.* **217**, 111883 (2024).
4. Okunogbe, A., Nugent, R., Spencer, G., Ralston, J. & Wilding, J. Economic impacts of overweight and obesity: current and future estimates for eight countries. BMJ Glob. Health **6**, https://doi.org/10.1136/bmjgh-2021-006351 (2021).
5. Alfaris, N., Alqahtani, A. M., Alamuddin, N. & Rigas, G. Global Impact of Obesity. *Gastroenterol. Clin. North Am.* **52**, 277–293 (2023).
6. Cheng, L. et al. Brown and beige adipose tissue: a novel therapeutic strategy for obesity and type 2 diabetes mellitus. *Adipocyte* **10**, 48–65 (2021).
7. Whitehead, A. et al. Brown and beige adipose tissue regulate systemic metabolism through a metabolite interorgan signaling axis. *Nat. Commun.* **12**, 1905 (2021).
8. Shao, M. et al. ZFP423 controls EBF2 coactivator recruitment and PPARγ occupancy to determine the thermogenic plasticity of adipocytes. *Genes Dev.* **35**, 1461–1474 (2021).
9. Fenzl, A. & Kiefer, F. W. Brown adipose tissue and thermogenesis. *Horm. Mol. Biol. Clin. Investig.* **19**, 25–37 (2014).
10. Cypess, A. M. et al. Activation of human brown adipose tissue by a β3-adrenergic receptor agonist. *Cell Metab.* **21**, 33–38 (2015).
11. Cero, C. et al. β3-adrenergic receptors regulate human brown/beige adipocyte lipolysis and thermogenesis. JCI Insight **6**, https://doi.org/10.1172/jci.insight.139160 (2021).
12. Shamsi, F., Wang, C.-H. & Tseng, Y.-H. The evolving view of thermogenic adipocytes—ontogeny, niche and function. *Nat. Rev. Endocrinol.* **17**, 726–744 (2021).
13. Hibi, M. et al. Brown adipose tissue is involved in diet-induced thermogenesis and whole-body fat utilization in healthy humans. *Int. J. Obes.* **40**, 1655–1661 (2016).
14. An, R., Ji, M. & Zhang, S. Global warming and obesity: a systematic review. *Obes. Rev.* **19**, 150–163 (2018).
15. Kajimura, S., Spiegelman, B. M. & Seale, P. Brown and beige fat: physiological roles beyond heat generation. *Cell Metab.* **22**, 546–559 (2015).
16. Wang, W. & Seale, P. Control of brown and beige fat development. *Nat. Rev. Mol. Cell Biol.* **17**, 691–702 (2016).
17. Dempersmier, J. et al. Cold-inducible Zfp516 activates UCP1 transcription to promote browning of white fat and development of brown fat. *Mol. Cell* **57**, 235–246 (2015).
18. Sambeat, A. et al. LSD1 interacts with Zfp516 to promote UCP1 transcription and brown fat program. *Cell Rep.* **15**, 2536–2549 (2016).
19. McClements, D. J. & Grossmann, L. A brief review of the science behind the design of healthy and sustainable plant-based foods. *npj Sci. Food* **5**, 17 (2021).
20. Hu, W. -j et al. Recent advances in Artemisia argyi Lev. et vant. polysaccharides: extractions, purifications, structural characteristics, pharmacological activities, and existing and potential applications. *Int. J. Biol. Macromol.* **279**, 135250 (2024).
21. Han, Y. et al. Artemisiae argyi water extract alleviates obesity-induced metabolic disorder. *Curr. Issues Mol. Biol.* **44**, 6158–6171 (2022).
22. Zhan, H. et al. Effects of Lactiplantibacillus plantarum WLPL01 fermentation on antioxidant activities, bioactive compounds, and flavor profile of Artemisia argyi. *Food Biosci.* **49**, 101908 (2022).
23. Park, S. H. et al. A phase 2, multi-center, randomized, double-blind, parallel-group trial to evaluate the efficacy and safety of CKD-495 in patients with acute and chronic gastritis. *Can. J. Gastroenterol. Hepatol.* **2025**, 2702089 (2025).
24. Li, Y., Li, Y., Fang, T., Feng, X. & Gao, D. Impact of processing methods and storage on the chemical composition of Artemisia argyi essential oil. *Ind. Crops Prod.* **229**, 121024 (2025).
25. Yang, M.-T. et al. Authentication, phytochemical characterization and anti-bacterial activity of two Artemisia species. *Food Chem.* **333**, 127458 (2020).
26. Zhang, Z. et al. In vivo anti-hepatitis B activity of Artemisia argyi essential oil-loaded nanostructured lipid carriers. Study of its mechanism of action by network pharmacology and molecular docking. *Phytomedicine* **116**, 154848 (2023).
27. Erdenebileg, S. et al. Artemisia argyi ethanol extract ameliorates nonalcoholic steatohepatitis-induced liver fibrosis by modulating gut microbiota and hepatic signaling. *J. Ethnopharmacol.* **333**, 118415 (2024).
28. Chen, L. L., Zhang, H. J., Chao, J. & Liu, J. F. Essential oil of Artemisia argyi suppresses inflammatory responses by inhibiting JAK/STATs activation. *J. Ethnopharmacol.* **204**, 107–117 (2017).
29. Yu, Z. et al. Itaconate alleviates diet-induced obesity via activation of brown adipocyte thermogenesis. *Cell Rep.* **43**, 114142 (2024).
30. Wang, S. et al. SOX4 facilitates brown fat development and maintenance through EBF2-mediated thermogenic gene program in mice. *Cell Death Differ.* **32**, 447–465 (2025).
31. Boström, P. et al. A PGC1-α-dependent myokine that drives brown-fat-like development of white fat and thermogenesis. *Nature* **481**, 463–468 (2012).
32. Gulyaeva, O., Dempersmier, J. & Sul, H. S. Genetic and epigenetic control of adipose development. *Biochim. Biophys. Acta Mol. Cell Biol. Lipids* **1864**, 3–12 (2019).
33. Wang, X. et al. DDB1 prepares brown adipocytes for cold-induced thermogenesis. *Life Metab.* **1**, 39–53 (2022).
34. Lee, H. J. et al. Endothelial cell-derived stem cell factor promotes lipid accumulation through c-Kit-mediated increase of lipogenic enzymes in brown adipocytes. *Nat. Commun.* **14**, 2754 (2023).
35. Inoue, S. I. et al. Short-term cold exposure induces persistent epigenomic memory in brown fat. *Cell Metab.* **36**, 1764–1778.e1769 (2024).
36. Hanssen, M. J. et al. Short-term cold acclimation recruits brown adipose tissue in obese humans. *Diabetes* **65**, 1179–1189 (2016).
37. Schulze, M. B. & Stefan, N. Metabolically healthy obesity: from epidemiology and mechanisms to clinical implications. *Nat. Rev. Endocrinol.* **20**, 633–646 (2024).
38. Blüher, M. Obesity: global epidemiology and pathogenesis. *Nat. Rev. Endocrinol.* **15**, 288–298 (2019).
39. Yu, D., Huang, N. N. & Du, X. W. Review of the Chemical Composition and Biological Activities of Essential Oils from Artemisia Argyi, Artemisia Princeps, and Artemisia Montana. *Curr. Top. Med. Chem.* **23**, 1522–1541 (2023).
40. Liu, Y. et al. From longevity grass to contemporary soft gold: Explore the chemical constituents, pharmacology, and toxicology of Artemisia argyi H.Lév. & vaniot essential oil. *J. Ethnopharmacol.* **279**, 114404 (2021).
41. Cypess, A. M. et al. Identification and importance of brown adipose tissue in adult humans. *N. Engl. J. Med.* **360**, 1509–1517 (2009).
42. Betz, M. J. & Enerbäck, S. Targeting thermogenesis in brown fat and muscle to treat obesity and metabolic disease. *Nat. Rev. Endocrinol.* **14**, 77–87 (2018).
43. Kazak, L. et al. A creatine-driven substrate cycle enhances energy expenditure and thermogenesis in beige fat. *Cell* **163**, 643–655 (2015).
44. Shin, H. et al. Lipolysis in brown adipocytes is not essential for cold-induced thermogenesis in mice. *Cell Metab.* **26**, 764–777.e765 (2017).

45. Li, R. et al. Anti-obesity effects of capsaicin and the underlying mechanisms: a review. *Food Funct.* **11**, 7356–7370 (2020).
46. Li, Y. J. et al. Aurantio-obtusin ameliorates obesity by activating PPARα-dependent mitochondrial thermogenesis in brown adipose tissues. *Acta Pharm. Sin.* **44**, 1826–1840 (2023).
47. Andreadis, P. et al. Semaglutide for type 2 diabetes mellitus: a systematic review and meta-analysis. *Diabetes. Obes. Metab.* **20**, 2255–2263 (2018).
48. Chouchani, E. T. et al. Mitochondrial ROS regulate thermogenic energy expenditure and sulfenylation of UCP1. *Nature* **532**, 112–116 (2016).
49. Niemann, B. et al. Apoptotic brown adipocytes enhance energy expenditure via extracellular inosine. *Nature* **609**, 361–368 (2022).
50. Xie, Y. Y. et al. Pygo2 regulates adiposity and glucose homeostasis via β-Catenin-Axin2-GSK3β signaling pathway. *Diabetes* **67**, 2569–2584 (2018).

Acknowledgements

We thank Dr. Jiahuai Han (Xiamen University) for providing Flag/HA-XM plasmids. We also thank Yaying Wu, Zheni Xu, and Dr. Changchuan Xie (School of Life Sciences, Xiamen University) for metabolic cage analysis. We would like to acknowledge the Xiamen University Laboratory Animal Center for their support in mouse breeding and the technical assistance provided by the rest of the W.H.L. laboratory staff.

Author contributions

S.W. and J.Z. designed the study, performed the data analysis, and wrote the initial manuscript. S.W., S.-L.L., and S.-T.L. carried out most of the experimental work and corrected the draft. F.-A.X. conducted bioinformatics analyses of the RNA-seq datasets and serum non-targeted metabolomics. T.H., K.C., W.-L.X., and Z.-R.H. were involved in the mouse experiments. S.-L.L., W.-H.L., Z.-R.H., and H.-Q.C. supervised the project, revised the manuscript and provided fundings. W.-H.L., as the guarantor, had full access to the study data and is accountable for ensuring the integrity of the data and the accuracy of the analysis. All data were generated internally, and no paper mill services were used. All authors confirm their accountability for all aspects of the work, ensuring its integrity and accuracy.

Competing interests

The authors declare no competing interests.

Additional information

Supplementary information The online version contains supplementary material available at https://doi.org/10.1038/s41538-025-00633-2.

Correspondence and requests for materials should be addressed to Jian Zhang or Weihua Li.